Published in final edited form as:

Cells Tissues Organs. 2019 ; 207(2): 97–113. doi:10.1159/000503280.

Investigating the Osteoinductive Potential of a Decellularized Xenograft Bone Substitute

Daniel N. Bracey[1,*], **Alexander H. Jinnah**[1,*,†], **Jeffrey S. Willey**[2], **Thorsten M. Seyler**[3], **Ian D. Hutchinson**[4], **Patrick W. Whitlock**[5], **Thomas L. Smith**[1], **Kerry A. Danelson**[1], **Cynthia L. Emory**[1], **Bethany A. Kerr**[1,6,7,†]

[1]Wake Forest Baptist Medical Center, Orthopaedic Surgery, Winston Salem, NC, USA

[2]Wake Forest Baptist Medical Center, Radiation Oncology, Winston Salem, NC, USA

[3]Duke University, Orthopaedic Surgery, Durham, NC, USA

[4]Albany Medical Center, Orthopaedic Surgery, Albany, NY, USA

[5]Cincinnati Children's Hospital, Orthopaedic Surgery, Cincinnati, OH, USA

[6]Virginia Tech-Wake Forest University School for Bioengineering and Sciences, Winston Salem, NC, USA

[7]Wake Forest School of Medicine, Cancer Biology, Winston Salem, NC, USA

Abstract

Bone grafting is the second most common tissue transplantation procedure worldwide. One of the alternative methods for bone repair under investigation is a tissue-engineered bone substitute. An ideal property of tissue-engineered bone substitutes is osteoinductivity, defined as the ability to stimulate primitive cells to differentiate into a bone-forming lineage. In the current study, we use a

† Corresponding Authors Alexander H. Jinnah, M.D., Wake Forest Baptist Medical Center Orthopaedic Surgery, 1 Medical Center Blvd, Winston-Salem, NC, 27157, USA, Tel: 336-716-4025, Fax: 336-716-6110, ajinnah@wakehealth.edu, Bethany A. Kerr, Ph.D., Wake Forest School of Medicine Cancer Biology, 1 Medical Center Blvd, Winston-Salem, NC, 27157, USA, Tel: 336-716-0320, Fax: 336-716-0255, bkerr@wakehealth.edu.

*Co-first authors

8.5.·Author Contributions

Dr. Jinnah and Dr. Bracey had substantial contributions to the conception, acquisition, analysis, and interpretation of the work. Together they drafted the original manuscript and assisted with ongoing revisions. Dr. Willey contributed to analysis and interpretation of data and critical revisions to the manuscript. Dr. Seyler substantially contributed to the conception and design of the work and critical revisions to the manuscript. Dr. Hutchinson substantially contributed to the conception and design of the work and critical revisions to the manuscript. Dr. Whitlock substantially contributed to the conception and design of the work, interpretation of data, and critical revisions to the manuscript. Dr. Smith substantially contributed to the conception and design of the work, analysis of data, and critical revisions to the manuscript. Dr. Danelson substantially contributed to the analysis of the work and critical revisions to the manuscript. Dr. Emory substantially contributed to the interpretation of the work and critical revisions to the manuscript. Dr. Kerr substantially contributed to the conception and design of the work, analysis, interpretation of data, and critical revisions to the manuscript. All authors approved the final version of the manuscript for publication and agreed to be accountable for all aspects of the work.

8.·Statements

8.2.·Statement of Ethics

All animal experiments conform to internationally accepted standards, and the study protocol was approved by the Wake Forest School of Medicine IACUC.

8.3.·Disclosure Statement

Dr. Patrick Whitlock has a patent which covers the intellectual property associated with the decellularization protocol used in this work. Patent #: US20070248638A1.

decellularization and oxidation protocol to produce a porcine bone scaffold and examine whether it possesses osteoinductive potential and can be used to create a tissue-engineered bone microenvironment. The decellularization protocol was patented by our lab and consists of chemical decellularization and oxidation steps using combinations of deionized water, trypsin, antimicrobials, peracetic acid (PAA), and triton-X100. To test if the bone scaffold was a viable host, pre-osteoblasts were seeded and analyzed for markers of osteogenic differentiation. The osteoinductive potential was observed *in vitro* with similar osteogenic markers being expressed in pre-osteoblasts seeded on the scaffolds and demineralized bone matrix. To assess these properties *in vivo*, scaffolds with and without pre-osteoblasts pre-seeded were subcutaneously implanted in mice for four weeks. MicroCT scanning revealed 1.6-fold increased bone volume to total volume ratio and 1.4-fold increase in trabecular thickness in scaffolds after implantation. The histological analysis demonstrates new bone formation and blood vessel formation with pentachrome staining demonstrating osteogenesis and angiogenesis, respectively, within the scaffold. Furthermore, CD31+ staining confirmed the endothelial lining of the blood vessels. These results demonstrate that porcine bone maintains its osteoinductive properties after the application of a patented decellularization and oxidation protocol developed in our laboratory. Future work must be performed to definitively prove osteogenesis of human mesenchymal stem cells, biocompatibility in large animal models, and osteoinduction/osseointegration in a relevant clinical model *in vivo*. The ability to create a functional bone microenvironment using decellularized xenografts will impact regenerative medicine, orthopaedic reconstruction, and could be used in the research of multiple diseases.

Keywords

bone scaffold; tissue engineering; osteoinductivity; bone microenvironment; angiogenesis

2. Introduction

Regeneration and healing of critical bone defects resulting from high energy trauma, infection, necrosis, or tumor resection remain a major clinical challenge for orthopaedic surgeons [Calori et al., 2011; Kolambkar et al., 2011; Fassbender et al., 2014; Oryan et al., 2017]. The local biology in these defects is disrupted, rendering the self-regenerative healing cascade insufficient, and thus, conventional reparative techniques lead to nonunions, malunions, and osteomyelitis [Oryan et al., 2014; Oryan et al., 2017]. The gold standard treatment for a traumatic bone defect is the use of autologous bone graft; however, due to the associated morbidity and lack of adequate bone stock/donor sites, alternative grafts are commonly used. Alternative bone grafts include allografts and tissue-engineered bone substitutes [Calori et al., 2011; Roddy et al., 2018]. Allograft use risks disease transmission and has limited availability from young, healthy donors [De Long et al., 2007; Campana et al., 2014]. Consequently, there is increased interest in tissue-engineered bone substitutes [Wanschitz et al., 2007; Pina et al., 2017; Shahi et al., 2018; Iaquinta et al., 2019].

The ideal tissue-engineered bone substitute will be osteoconductive, osteoinductive, and osteogenic [Calori et al., 2011; Oryan et al., 2017]. Osteoconductivity is the ability for the bone graft to allow osseous growth on the surface or within its pores [Khan et al., 2005].

Osteogenic grafts retain living bone cells [Khan et al., 2005]. Osteoinductivity is the ability to stimulate progenitor cells to differentiate into a bone-forming cell lineage [Albrektsson and Johansson, 2001; Khan et al., 2005]. Tissue-engineered bone replacements can be manufactured with customized structures for osteoconductivity and pre-seeded with osteogenic cells to establish osteogenicity prior to implantation [Zimmermann and Moghaddam, 2011]. Osteoinductivity, however, requires the construct to induce cell differentiation and therefore is more difficult to recreate [Albrektsson and Johansson, 2001; Fielding and Bose, 2013; Hsu et al., 2013; Oryan et al., 2017]. Xenograft derived tissue-engineered constructs are one potential way to utilize the natural osteoinductive properties of native bone. One ideal species for xenotransplantation is swine due to physiologic compatibility with humans [Pierson et al., 2009; Wancket, 2015]. However; the presence of the alpha-gal epitope in porcine tissue can induce a severe inflammatory response in human hosts [Cooper et al., 2015; Vadori and Cozzi, 2015]. Our laboratory developed a decellularization protocol that sterilizes porcine soft tissues and removes the porcine DNA, including the alpha-gal epitope [Whitlock et al., 2007; Whitlock et al., 2012; Seyler et al., 2017]. We have applied this process to porcine cancellous bones and demonstrated that the construct was successfully decellularized and maintained native structural properties, therefore preserving the construct's osteoconductivity [Bracey et al., 2018; Bracey et al., 2019]. This research project aimed to determine whether the osteoinductive potential of the porcine-derived bone scaffold would be maintained following application of our patented decellularization and oxidation technique in *in vitro* and *in vivo* models.

3. Materials and Methods

Bone Scaffold Decellularization

To generate the bone scaffolds, porcine tissues were processed by decellularization and oxidation using methods previously described [Whitlock et al., 2012; Seyler et al., 2017; Bracey et al., 2018; Bracey et al., 2019]. Porcine bones were obtained from City Packing Company slaughterhouse (Burlington, NC, USA) as discarded tissue from female pigs (Sus scrofa domesticus) aged between 3–4 years old. Briefly, the cancellous bone was harvested from the distal metaphysis of porcine femurs and subjected to chemical decellularization and oxidation using combinations of deionized water, trypsin, antimicrobials, peracetic acid (PAA), and triton-X100. Scaffolds were lyophilized and frozen at −80°C until further use. Scaffolds were cut to 1 cm diameter, and the thickness ranged between 0.2 to 0.5 cm. The bone scaffolds were not decalcified at any point during this process.

Cell Culture

C2C12 and MC3T3-E1 cell lines were chosen for indirect quantification of the bone scaffold's osteoinductive potential. C2C12 (CH3 genetic background, ATCC® CRL-1772™, Rockville, MD) is a mouse myoblast cell line that differentiates into osteoblasts in the presence of BMP-2 and is commonly used in osteoinduction studies [Katagiri et al., 1994; Han et al., 2003; Yang et al., 2011; Shi et al., 2012; Ansari et al., 2013]. C2C12 cells were grown in DMEM media supplemented with 10% FBS. MC3T3-E1 cells (ATCC® CRL-2593™, Rockville, MD) were chosen as a second cell line to confirm the bone scaffold's osteoinductive potential. These cells are an osteoblast precursor derived from

C57BL/6 mice and have previously been used to study osteoinductive potential as well [Shuang et al., 2016; Araujo-Gomes et al., 2018]. MC3T3-E1 cells were grown in αMEM media supplemented with 10% FBS and sodium pyruvate. The percentage of C2C12 and MC3T3-E1 cells attached to the bone scaffolds after 3 hours were 50% and 30%, respectively. In our subsequent characterization experiments, cells were given at least 24 hours to attach prior to any manipulation or media change.

Osteogenic Differentiation of C2C12 Cells

Bone scaffolds or commercial grade cancellous demineralized bone matrix (DBM, Musculoskeletal Transplant Foundation, Edison NJ) sheets (n=49 per group) were seeded with 1×10^6 C2C12 cells suspended in 100 μl cell culture media. DBM is commonly used in clinical applications because of its reported osteoconductive and osteoinductive potential. Constructs were moved into large Petri dishes, covered with DMEM + 10% FBS media, and returned to the incubator. As a negative control, cells were also seeded onto gelfoam sponges (Cardinal Health) which are assumed to have no or very limited biologic activity.

Constructs were incubated for 24 hours to allow cells to attach to the matrix. Sub-samples from each group (n=7) were taken for analysis while the remaining were separated for continued incubation in 2 different media: 1) “Osteogenic Media (OM)” [Shui et al., 2013; Sondag et al., 2013; Yu et al., 2013; Hupkes et al., 2014] consisting of DMEM with 10 mM β-Glycerophosphate and 50 μg/mL ascorbic acid or 2) “BMP-2 Enriched Media” [Han et al., 2003; Feichtinger et al., 2011; Yang et al., 2011; Ansari et al., 2013] consisting of the osteogenic media supplemented with 100 ng/mL BMP-2 (recombinant human BMP-2, 355-BM-050, R&D Systems) were added on Day 2. Media was replaced every three days. The osteogenic media provided an environment supportive of osteogenic differentiation while the BMP-2 enriched media served as a positive control to drive cells towards osteoblastic lineage. Constructs (n=7) were harvested from each group at days 1, 3, 7, and 15 for analysis of cell proliferation and osteogenic differentiation.

Cell Viability and Proliferation on Scaffolds

At each time point, constructs (n=2) from each group (n=7) were removed from their respective dishes and individually rinsed with warm, sterile PBS. Constructs were then transferred to chamber slides and incubated with the Live/Dead® Viability/Cytotoxicity Kit (Molecular Probes, Eugene, OR) according to manufacturer’s instructions. Specimens were immediately imaged on a fluorescence confocal microscope (Zeiss Axiovert 100 M) to render cross-sectional 2D images as well as projected 3D images. Live cells are labeled with the green calcein-AM fluorophore, and dead cells are labeled with the red ethidium homodimer-1 fluorophore. Fluorescence was quantified using NIH Image J.

DNA content was quantified from separate constructs (n=3) in each group to estimate cell number and proliferation. Samples were flash-frozen in liquid nitrogen, homogenized with a sterilized tissue press, and lysed in 1 mL mammalian protein extraction reagent (M-PER®, ThermoScientific, Waltham, MA). Samples were centrifuged 15 minutes at 13.2 kRPM, and supernatants were collected for analysis. DNA content was measured with Quant-iT™

PicoGreen® dsDNA Assay Kit (Thermo Scientific) according to the manufacturer's instructions.

Scanning Electron Microscopy and Scaffold Histology

Cell attachment, morphology, and surface distribution were characterized by electron microscopy. Constructs that had been used for live/dead staining (n=2) were gently washed with warmed sterile PBS and fixed in 2.5% SEM-grade glutaraldehyde for 3 hours. Fixed constructs were rinsed in water for 30 minutes and dehydrated through ethanol (50%, 70%, 80%, 90%, 95%, and 100%) for 20 minutes each. Constructs were then transferred in 100% ethanol to a CO_2 critical point dryer. Constructs were then mounted on aluminum stubs with double-sided carbon tape and gold sputter-coated at 30 mTorr. Specimens were imaged on a Hitachi S-2600 scanning electron microscope (SEM).

Constructs (n=2) from each group were removed from dishes, fixed in 10% formalin for 48 hours, decalcified with Immunocal® (Decal Chemical Cort, Tallman, NY) for 3–5 days, processed and embedded in paraffin. Sections were mounted and stained with hematoxylin and eosin (H&E) or 4',6-diamidino-2-phenylindole (DAPI) mounting media (ProLong® Gold Antifade Mountant, Thermo Scientific). Representative light micrographs were captured with the Olympus VS-110 Virtual Imaging System and fluorescent micrographs with a Zeiss Axioplan2 system. DAPI fluorescence was quantified with NIH Image J.

Alkaline Phosphatase Enzyme Assay

The alkaline phosphatase (ALP) enzyme activity was measured from individual constructs, that were also used for DNA analysis (n=3) using methods previously described [Liu et al., 2008; Stiehler et al., 2010; Thibault et al., 2010; Arca et al., 2011; Marcos-Campos et al., 2012; Kerr et al., 2013; Shi et al., 2013]. Phosphatase enzyme-substrate, p-nitrophenyl phosphate (pNPP, Thermo Scientific), was prepared by dissolving the pNPP tablet in dH_2O buffered with diethanolamine (DEA, Thermo Scientific) and 0.5 mM MgC_{l2}. 150 µl of the supernatant dilution from each sample was added to 325 µl enzyme-substrate and incubated in a 37°C water bath for 30 minutes. The reaction was halted by the addition of 25 µl 2M NaOH. Each reaction was read in triplicate by loading 150 µl from each tube into 96 well plates and measuring absorbance at 405 nm on a microplate reader (Spectra Max 340 PC). p-Nitrophenol (p-NP) standards were prepared in dH_2O to generate a standard curve and derive p-NP produced from each substrate reaction. Each reaction was read in triplicate by loading 150 µl from each tube into 96 well plates and measuring absorbance at 405 nm on a microplate reader (Spectra Max 340 PC) [Arca et al., 2011; Hashimoto et al., 2011; Kouroupis et al., 2013].

Alkaline Phosphatase Immunohistochemistry

Immunohistochemistry (IHC) was performed on the constructs that were fixed for histological evaluation (n=2) with an anti-Placental ALP (Abcam ab16695, Cambridge, United Kingdom) primary antibody that reacts with cell membrane-bound enzyme. Secondary biotin-conjugated anti-rabbit antibody (BioGenex, Freemont, CA) was linked to HRP (horseradish peroxidase) and developed with DAB (diaminobenzidine) substrate (Vector, Burlingame, CA). Slides were counterstained with Mayer's Hematoxylin.

Differentiation of MC3T3-E1 cells

MC3T3-E1 cells (1×10^6) suspended in 250 μL of cell culture media were seeded and incubated on scaffolds (n=18) for 1 hour before being submerged in 750 μL of α-MEM and incubated at 37° C for 7 days. Control monolayers (n=9) of 1×10^6 cells plated on 10 μg/mL collagen type I (Sigma) were also incubated at 37° C for 7 days in α-MEM. Cell culture media was changed every 3 days.

Subcutaneous Implantation of Scaffolds

To demonstrate cell viability and osteoinductivity *in vivo,* the scaffolds were either pre-seeded (n=25) with MC3T3-E1 cells (1×10^6 suspended in 50 μL α-MEM) or not pre-seeded with any cells (n=15). These scaffolds were then subcutaneously implanted in the right flank of 7-week-old C57BL/6 male mice (Jackson Labs, Bar Harbor ME) for four weeks under a Wake Forest School of Medicine IACUC Protocol #A16–197 (one scaffold per mouse). During implantation, mice were anesthetized with ketamine/xylazine and given buprenorphine as postsurgical analgesia. Incision sites were closed with staples which were removed one week postoperatively. Mice were maintained on standard chow in standard housing. Upon experimental termination, mice were euthanized by carbon dioxide inhalation followed by cervical dislocation.

Micro-computed Tomography (microCT)

All scaffolds underwent micro-computed-tomography (microCT) scanning (TriFoil Imaging Triumph II PET/CT) before cell seeding and implantation. Upon explantation, constructs were either snap-frozen in liquid nitrogen and ground to extract RNA (see below) or placed in 10% formalin to undergo microCT scanning to assess new bone formation (n=12 pre-seeded, n=7 unseeded). After 24 hours of fixation at 4oC on a shaker, scaffolds were placed in PBS. For scaffolds that underwent microCT scanning (pre and post-implantation), scaffolds were removed from the PBS, placed in a polystyrene mold, and scanned on a TriFoil Triumph II microPET/CT with X-O CT system in the Wake Forest SOM Translational Imaging Program Shared Resource. Images were obtained at 80 peak kilovoltage and 140 μA, and 1024 projections were acquired over 360° rotation over 3.96 minutes. The field of view was 84.57 mm (1.4X magnification). CT scans were reconstructed on the TriFoil Triumph X-O CT software version 5.2.0.0 using a back-projection image with a matrix of 512 and a voxel spacing of 170 μm. Three-dimensional data were processed and rendered (isosurface/maximum intensity projections) with a voxel size of 0.17 mm in each dimension and analyzed using the MicroView 3D Image Viewer and Analysis Tool (Parallax Innovations, Ilderton, ON, Canada). A standardized region of interest (ROI) was used to encompass the entire scaffold area and the Bone Analysis tool run to obtain the Stereology bone parameters including bone volume/total volume ratio (BV/TV), trabecular spacing (Tb.Sp), bone surface/bone volume (BS/BV), and trabecular thickness (Tb.Th). Thresholds were set at 1200 based on the Isosurface Tool and the bone and water ADU set based on values generated by scanning a phantom. New bone formation was assessed through the change in BV/TV and Tb.Th between pre and post-implantation scans.

Implanted Scaffold Histology and Immunohistochemistry

Fixed scaffolds that underwent microCT scanning were subsequently decalcified in 14% neutral, saturated EDTA for 7–14 days. Samples were processed and embedded in paraffin. Sections were stained with Russel-Movat Pentachrome (American MasterTech Scientific Inc; St. Lodi, CA). Tartrate resistant acid phosphatase (TRAP) staining was performed as previously described [McCabe et al., 2011]. IHC was performed using a primary antibody against CD31 (Abcam ab28364) to identify angiogenesis. Slides were scanned using a Hamamatsu NanoZoomer by the Virtual Microscopy Core.

qPCR Analysis

RNA was isolated from the scaffolds (n = 13 preseeded, n = 8 unseeded) by grinding in liquid nitrogen followed by lysis in Qiazol Reagent (RNeasy Microarray Tissue Mini Kit, QIAGEN, Hilden, Germany), and then RNA purified following the manufacturer instructions. RNA from monolayers was also isolated following manufacturer instructions using the RNeasy Mini Kit. cDNA was produced through reverse transcription using High Capacity cDNA Reverse Transcription Kit (Applied Biosystems) and then analyzed for gene expression of different osteoblast markers using quantitative PCR. Target gene expression was normalized to the [McCabe et al., 2011]housekeeping gene 18S ribosomal RNA (rRNA). Primer sequences are available in Table 1. Relative gene expression was quantified by using the $2^{-\Delta\Delta Ct}$ methodology originally described by Livak and Schmittgen [Livak and Schmittgen, 2001].

Statistical Analysis

Multiple group comparisons were performed using two-way ANOVA with Tukey's multiple comparison tests for experiments comparing treatments and construct, one-way ANOVA with Tukey's post-test were used for experiments over time, t-tests were performed on independent means when comparing two groups, and paired t-tests were used when comparing paired groups using GraphPad Prism 7. Statistical significance was determined when α-error<0.05.

4. Results

Scaffolds Support C2C12 Pre-Osteoblast Survival

Bone scaffolds were generated from the femur of female pigs and decellularized through a patented process as described in prior publications [Seyler et al., 2017; Bracey et al., 2018; Bracey et al., 2019]. The resulting scaffolds are free of DNA and the alpha-gal epitope but retain the native bone structure. Scaffolds used in our experiments had an average porosity of 75.8% (range: 58.7% - 90.3%) and an average scaffold surface are to total volume ratio of 3.1 mm-1 (range: 1.1 – 8.5). To assess whether the scaffold could support osteoblast growth, C2C12 pre-osteoblasts were seeded on bone scaffolds, demineralized bone matrix, or gel foam constructs. C2C12 pre-osteoblasts proliferated on scaffolds and deposited extracellular matrix (ECM) components. Three-dimensional images of Live/Dead staining demonstrated circumferential cell attachment evenly around the pores. In all constructs, the live (green) signal increased during incubation (Figure 1). Dead (red) signal was high on day 1, likely

due to early contact inhibition after seeding constructs at a high cell density. Additionally, all constructs displayed autofluorescence in the red channel as shown in the Blank images (Figure 1), which was subtracted from the red signal in the later graphs. For all constructs, BMP-2 treatment resulted in the highest ratio of live/dead cells on day 15 (DBM: 1.2-fold; gelfoam: 6.0-fold; scaffold: 6.2-fold) compared with day 1 (Figure 1). To assess proliferation on the constructs, DNA content was measured on the three constructs over 15 days in the presence or absence of 100 ng/mL BMP-2 treatment starting on day 2 to induce osteoblast differentiation. DNA content on DBM was greater than scaffolds at every time point, indicating higher cell density (Figure 2). BMP-2 treatment had no consistent effect on cell proliferation. Cells seeded on the scaffold proliferated, as demonstrated by increased DNA at each time point with a 6.5-fold increase between days 1 and 15. The differences were significant between day 1 and 15 ($p<0.01$) and day 3 and 15 ($p=0.01$). Similarly, DNA mass on DBM increased at each time point as well (Figure 2), while the gelfoam constructs demonstrated increased DNA content at day 7 with a decrease at day 15. To confirm cell numbers and adhesion to the constructs, C2C12 seeded DBM and decellularized bone scaffolds were examined. DAPI and H&E staining (Figure 3) confirmed higher cell density on DBM relative to scaffolds indicating that the increased cell proliferation is occurring in cells attached to the constructs. DAPI fluorescence was 1.4-fold higher in the DBM constructs compared with the scaffolds. Finally, scanning electron microscopy confirmed C2C12 adhesion to and spreading on the constructs. Interestingly, similar densities of cell distribution were noted on DBM samples and scaffolds at day 7 and 15 (Figure 4). ECM was deposited uniformly at later time points, and BMP-2 did not change cell morphology, density, or distribution on matrices. Thus, the decellularized bone scaffolds were equally capable of supporting pre-osteoblast adhesion and survival underscoring the osteogenic nature of the scaffolds.

Decellularized Bone Scaffolds Enhance Pre-Osteoblast Differentiation

To examine the osteoinductive capacity of the decellularized bone scaffolds, C2C12 pre-osteoblast differentiation on the constructs was compared. C2C12 cells were seeded onto either DBM, bone scaffolds, or Gelfoam and grown for up to fifteen days in the presence or absence of BMP-2 starting on day 2. Molecular assays demonstrated that cells seeded on decellularized bone scaffolds had greater ALP enzyme activity at day 7 (~5 and 7-fold) and day 15 (~4 and 14-fold) ($p<0.0001$) compared to cells seeded on DBM or gelfoam constructs, respectively (Figure 5). BMP-2 increased ALP activity significantly on scaffolds (day 7: ~40fold ($p<0.0001$) and day 15: ~64-fold ($p<0.0001$)), suggesting an additive effect on this matrix. ALP IHC staining increased at day 15 in C2C12 cells seeded on bone scaffolds and supported the above cell-specific enzyme activity findings (Figure 6). ALP staining demonstrates darker staining on the scaffolds compared with DBM in the presence or absence of BMP-2. Thus, the bone scaffolds support osteoblast differentiation of C2C12 cells.

To confirm the osteoinductive potential of the decellularized bone scaffolds, MC3T3-E1 pre-osteoblast cells were grown on the scaffolds. Compared to cells grown in a monolayer on collagen type I, MC3T3-E1 cells on the bone scaffolds expressed 2.5-fold higher RANKL

(*Tnfsf11*) and 2-fold higher *Bmp2* (Figure 7). Taken together, these results indicate that the bone scaffold possesses osteoinductive potential *in vitro*.

Implantation of Scaffolds in Syngeneic Mice Induces the Formation of a Bone Microenvironment

Based on the osteogenic and osteoinductive capabilities of the decellularized bone scaffold, we hypothesized that the seeded scaffold might be osteoconductive *in vivo*. MC3T3-E1 pre-osteoblasts were seeded on bone scaffolds and implanted subcutaneously in syngeneic mice. Unseeded scaffolds were implanted as controls. Upon removal, scaffolds were examined for changes in osteoblast differentiation gene expression. *In vivo* expression of *Alpl* (3.3-fold), *Bmp2* (10.3-fold), and *Bmp7* (3.9-fold) increased within the pre-seeded scaffolds relative to the unseeded scaffolds (Figure 8). RANKL (*Tnsfs11*) gene expression was equal between groups (data not shown). To assess changes in the bone structure and measure possible bone formation, microCT analysis was performed on seeded (n=9) and un-seeded (n=4) scaffolds (Figure 9). Representative microCT images of unseeded and pre-seeded scaffolds preimplantation and post-explantation are shown in Figure 9. Evaluation of new bone formation was performed by comparing the pre-implantation microCT scan to the post-explantation microCT scan. The average change in bone volume to total volume ratio (BV/TV) and trabecular thickness (Tb.Th) were then compared between the pre-seeded and unseeded groups. Increase in Tb.Th was seen in the pre-seeded scaffolds ($p=0.04$); however, no significant difference was identified in BV/TV ratio ($p=0.08$). Paired t-tests showed significantly increased BV/TV (1.6-fold, $p=0.0013$) and Tb.Th (1.4-fold, $p=0.0002$) after explantation when both groups are combined (n=13) indicating new bone formation, regardless of cell seeding prior to implantation (Figure 9). After removal, scaffolds were sectioned and analyzed for osteogenesis and angiogenesis. Pentachrome staining of the scaffolds displayed new bone formation within the pores of the scaffold in both groups (Figure 10A and 10C). To assess whether osteoclasts could be recruited to the scaffolds, staining for tartrate-resistant acid phosphatase (TRAP) was performed. Small TRAP-positive cells were seen within the pores and rare cells along the bone surface (Figure 10B and 10D). These cells likely represent osteoclast progenitor cells, although no mature osteoclasts were seen within the four-week time frame. Of note, pentachrome staining revealed apparent vascular-like structures (Figure 11A and 11C) within the scaffold. IHC analysis demonstrated positive CD31 staining of endothelial cells organized around a lumen and indicating angiogenesis within the decellularized bone scaffold (Figure 11B and 11D). These results demonstrated that the scaffold maintains osteoinductive potential following decellularization, due to its ability to recruit and stimulate cells down a bone-forming lineage *in vivo*. Further, implantation of the scaffold in a syngeneic host, even without pre-osteoblast seeding, can generate a bone microenvironment.

5. Discussion/Conclusion

Previously, our laboratory established a decellularization and oxidation technique using PAA that removes 98% of DNA when applied to porcine bone [Bracey et al., 2018; Bracey et al., 2019]. In this study, we demonstrate that this protocol preserves the native bone's osteoinductive potential in a decellularized scaffold. The decellularized bone scaffold

supported pre-osteoblast survival and differentiation comparable to DBM, a commercial product currently in clinical use with proven osteoinductive potential. Further, the bone scaffold supported the development of a bone microenvironment, including osteogenesis and angiogenesis. Furthermore, our scaffolds demonstrated an average porosity of about 75%, which is in line with the average porosity of natural cancellous bone (75–90%), and ideal for bone regeneration [Polo-Corrales et al., 2014; Chocholata et al., 2019]. Thus, the decellularized bone scaffold is osteoconductive and osteoinductive.

Control of osteogenesis *in vitro* and *in vivo* is integral to regenerative medicine applications in orthopaedic research. BMP-2 is one of the strongest stimulants of osteogenic differentiation in the pre-osteoblast cell lines used in our experiments [Katagiri et al., 1994; Han et al., 2003; Bormann et al., 2010; Miron et al., 2013; Qadir et al., 2015; Fu et al., 2017; Heo et al., 2018]. Concentrations as low as 100 ng/mL and 50 ng/mL were sufficient to promote osteogenic differentiation with increased ALP activity in MC3T3-E1 [Fu et al., 2017] and C2C12 [Han et al., 2003], respectively. However, few reports studied osteogenic differentiation of cells seeded onto xenograft-derived bone scaffolds [Arca et al., 2011; Hashimoto et al., 2011; Marcos-Campos et al., 2012; Kouroupis et al., 2013; Lu et al., 2013]. Hashimoto et al. demonstrated porcine hydroxyapatite contains osteoinductive properties and that these properties are maintained after processing [Hashimoto et al., 2011]. Similarly, Smith et al. found the osteoinductive properties were maintained in allografts following a decellularization and washing procedure [Smith et al., 2015]. However, Bormann et al. used a similar decellularization and oxidation protocol to ours with the addition of PAA on allografts and found the osteoinductive potential was not maintained [Bormann et al., 2010]. In the present study, we applied a decellularization and oxidation technique using PAA that removed 98% of the porcine DNA from the bone scaffolds [Bracey et al., 2018; Bracey et al., 2019]. Contrary to the findings by Borman et al. with human bone, our results demonstrate that the xenograft does indeed maintain osteoinductive potential after processing. C2C12 and MC3T3-E1 cells attached to the scaffold matrix, proliferated, and underwent osteogenic differentiation during the incubation period. The discrepancy between these studies outlines the variability between decellularization techniques as well as donor species. Bormann et al. reported that the donors ranged in both age (13–67 years) and gender, and ultimately concluded this could be a source of variability between the human-derived samples. These discrepancies may affect osteoinductive potential [Smith et al., 2017] and outline the importance of controlling environmental factors that may influence the quality of the donor bone, which is possible with the use of a xenograft.

Our *in vivo* microCT results demonstrated that there was equal osteogenesis identified in the pre-seeded and unseeded scaffolds. This finding suggests that the scaffold alone recruits the necessary cells for osteogenesis. Combining the microCT analysis and histologic assessment of the porcine bone scaffold *in vivo* demonstrated spontaneous new bone formation and angiogenesis. The identification of angiogenesis represents a critical finding due to the lack of vascularization being one of the major limitations associated with the use of tissue-engineered constructs during early bone regeneration [Muschler et al., 2004; Giannoni et al., 2010; Saran et al., 2014].

To create a humanized bone microenvironment, Hesami et al. utilized electrospun polycaprolactone scaffolds coated with calcium phosphate and seeded with human osteoblasts in the presence of BMP-7 [Hesami et al., 2014]. After 12 weeks, scaffolds contained hematopoietic and adipose cells resembling marrow. In a separate study, the electrospun scaffolds were coated in PRP and BMP-7 prior to implantation in a critical defect model for 12 weeks and were also able to form bone [Berner et al., 2012]. Another study of BMP-7 coated beta-tricalcium phosphate demonstrated new bone formation, differentiated osteoclast recruitment, and angiogenesis; however, it required twelve months of implantation in a critical defect within an existing bone [Reichert et al., 2012]. Our scaffold demonstrates the recruitment of osteogenic cells and extended implantation would be required to determine whether a more functional marrow similar to that described by the two groups would develop. BMP-2 coating of lyophilized type I collagen scaffolds also induced angiogenesis and osteogenesis in a critical defect model through a paracrine model in which osteoblasts secreted factors stimulating endothelial cell migration [Pearson et al., 2019]. In this model bone formation and angiogenesis was seen at 3 weeks in the bone defect, similar to our findings at 4 weeks of subcutaneous growth. Thus, BMP-2 secretion by osteoblasts may account for the angiogenesis into the subcutaneously implanted bone scaffold. In our model, we did not add exogenous BMP-7 or BMP-2 to the implanted scaffolds but we do demonstrate that the osteoblast cells culture on the bone scaffold express endogenous BMP-7 and BMP-2 which may drive osteoblast differentiation and bone formation.

BMP-7 or BMP-2 in combination with vascular endothelial growth factor increases angiogenesis in various constructs designed to function as bone grafts [Liu et al., 2014; Sharma et al., 2018]. Although we did not directly examine vascular endothelial growth factor secretion by MC3T3-E1 cells seeded on scaffolds, prior studies have demonstrated that multiple growth factors and mechanical stress induce vascular endothelial cell secretion by MC3T3-E1 [Tokuda et al., 2008; Nakai et al., 2009; Tokuda et al., 2011]. Interestingly, a BMP-2/7 heterodimer induces bone formation at a great rate than either isoform alone and is also able to induce osteoclastogenesis [Zhu et al., 2004; Sun et al., 2012; Zheng et al., 2012]. Thus, the expression of both BMPs by the preosteoblasts on the bone scaffold in our study may lead to the recruitment of both endothelial cells and TRAP-positive osteoclast progenitors.

The presence of angiogenesis signifies graft-host integration by the induction of inflammatory cytokines as part of the normal healing process [Stegen et al., 2015]. The recruitment of inflammatory cytokines promotes chondrogenesis, formation of hypertrophic cartilage, and then replacement by bone [Grosso et al., 2017]. It is reasonable to conclude that the presence of angiogenesis allowed for new bone formation due to the known importance angiogenesis has in bone repair and regeneration [Saran et al., 2014; Stegen et al., 2015]. Accordingly, Hirata et al. found that a BMP-2 soaked absorbable collagen sponge implanted in humans led to new bone formation lined by endothelial cells [Hirata et al., 2017]. Furthermore, Bhumiratana et al. implanted a clinically approved decellularized bovine trabecular bone seeded with adipose-derived stem cells into Yucatan minipig skull defects and concluded that angiogenesis and new bone formation occurred in parallel [Bhumiratana et al., 2016]. Thus, our decellularized bone scaffold represents a potential

tissue-engineered bone microenvironment capable of both angiogenesis and osteogenesis. The angiogenesis demonstrated in these experiments may be due to the complex inflammatory response between the decellularized scaffold and M1 and M2 macrophages, and IL-4. This has been previously demonstrated within decellularized bone scaffold implants [Zheng et al., 2018], but is beyond the scope of this investigation.

There are limitations to our study. First, clinical translation of *in vitro* and animal experiments is limited. However, we believe these experiments are a necessary step to determine the properties of this bone scaffold after undergoing the decellularization and oxidation procedure. Second, our *in vivo* experiments involve an ectopic subcutaneous implantation model, rather than an orthotopic bone void filling model. However, the purpose of these experiments was solely to determine the osteoinductive potential of this scaffold in an *in vitro* and *in vivo* environment. Thus, we used subcutaneous implantation as it is a common method for assessing intrinsic vascularization in mice [Chan et al., 2016; Chen et al., 2018; Wang et al., 2019], and has been used in our lab previously. It allows an easily accessible implant for explantation and allows a minimally invasive surgical procedure. Finally, a major limitation is using murine rather than human cell lines for these experiments, which limits immediate clinical translation. These cell lines, however, have been validated for the study of biomaterial osteoinductive potential previously [Qadir et al., 2015; Kanayama et al., 2017]. Despite these limitations, the decellularized porcine bone scaffold can be used in future experiments to assess its clinical and therapeutic utility.

Overall, our data demonstrate that a decellularization and oxidation technique applied to porcine metaphyseal bone preserves the osteoinductive potential of the bone. Previous literature identified that these properties are the most difficult to artificially create in tissue-engineered scaffolds and to maintain when processing bone scaffolds, therefore outlining the potential clinical impact of this construct. Future studies involving this xenograft will focus on placing the construct within a bone defect, identifying osseointegration, and comparing it to current standard treatments. These experiments will look at the effect of supplementing the scaffold with human mesenchymal stem cells as a step towards clinical translation. Furthermore, an *in vivo* analysis of inflammatory markers to confirm that the bone scaffold has no increased reactivity when compared to currently used clinical implants for large bone defects should be performed. Further research will determine whether this decellularized bone scaffold capable of osteoinductivity and osteogenesis is fully osteoconductive and able to function as a substitute bone microenvironment.

8.1. Acknowledgments

We would like to thank Ms. Eileen Elsner, Ms. Jiaozhong Cia, Mr. Koran Harris, and Dr. Lihong Shi for their help with tissue processing and animal handling throughout these experiments. We thank Brandi Bickford from the Virtual Microscopy Core for her assistance in slide scanning.

8.4. Funding Sources

We thank the Orthopaedic Research and Education Foundation (OREF) and AO Trauma North America for their contribution to the funding of this project through a Resident Clinician Scientist Research Grant to D.N.B.. We would also like to thank the Musculoskeletal Transplant Foundation (MTF) for their donation of human DBM samples at no cost. The animal experiments were supported by a CTSI Ignition Fund under the NIH/NCATS UL1 TR001420 grant to B.A.K. which also supports the shared resources at Wake Forest School of Medicine. B.A.K

was supported by grant from the NIH/NCI R00 CA175291. None of the funding sources have been given the manuscript to review. The funding bodies have been given periodic updates on our work.

9. References

Albrektsson T, Johansson C (2001) Osteoinduction, osteoconduction and osseointegration. Eur Spine J 10 Suppl 2: S96–101. [PubMed: 11716023]

Ansari S, Moshaverinia A, Pi SH, Han A, Abdelhamid AI, Zadeh HH (2013) Functionalization of scaffolds with chimeric anti-BMP-2 monoclonal antibodies for osseous regeneration. Biomaterials 34(38): 10191–10198. [PubMed: 24055525]

Araujo-Gomes N, Romero-Gavilan F, Garcia-Arnaez I, Martinez-Ramos C, Sanchez-Perez AM, Azkargorta M, Elortza F, de Llano JJM, Gurruchaga M, Goni I, Suay J (2018) Osseointegration mechanisms: a proteomic approach. Journal of biological inorganic chemistry : JBIC : a publication of the Society of Biological Inorganic Chemistry.

Arca T, Proffitt J, Genever P (2011) Generating 3D tissue constructs with mesenchymal stem cells and a cancellous bone graft for orthopaedic applications. Biomed Mater 6(2): 025006.

Berner A, Boerckel JD, Saifzadeh S, Steck R, Ren J, Vaquette C, Zhang JQ, Nerlich M, Guldberg RE, Hutmacher DW, Woodruff MA (2012) Biomimetic tubular nanofiber mesh and platelet rich plasma-mediated delivery of BMP-7 for large bone defect regeneration. Cell and tissue research 347(3): 603–612. [PubMed: 22277992]

Bhumiratana S, Bernhard JC, Alfi DM, Yeager K, Eton RE, Bova J, Shah F, Gimble JM, Lopez MJ, Eisig SB, Vunjak-Novakovic G (2016) Tissue-engineered autologous grafts for facial bone reconstruction. Science translational medicine 8(343): 343–383.

Bormann N, Pruss A, Schmidmaier G, Wildemann B (2010) In vitro testing of the osteoinductive potential of different bony allograft preparations. Archives of orthopaedic and trauma surgery 130(1): 143–149. [PubMed: 19529951]

Bracey DN, Seyler TM, Jinnah AH, Lively MO, Willey JS, Smith TL, Van Dyke ME, Whitlock PW (2018) A Decellularized Porcine Xenograft-Derived Bone Scaffold for Clinical Use as a Bone Graft Substitute: A Critical Evaluation of Processing and Structure. Journal of functional biomaterials 9(3).

Bracey DN, Seyler TM, Jinnah AH, Smith TL, Ornelles DA, Deora R, Parks GD, Van Dyke ME, Whitlock PW (2019) A porcine xenograft-derived bone scaffold is a biocompatible bone graft substitute: An assessment of cytocompatibility and the alpha-Gal epitope. Xenotransplantation: e12534.

Calori GM, Mazza E, Colombo M, Ripamonti C (2011) The use of bone-graft substitutes in large bone defects: any specific needs? Injury 42 Suppl 2: S56–63. [PubMed: 21752369]

Campana V, Milano G, Pagano E, Barba M, Cicione C, Salonna G, Lattanzi W, Logroscino G (2014) Bone substitutes in orthopaedic surgery: from basic science to clinical practice. J Mater Sci Mater Med 25(10): 2445–2461. [PubMed: 24865980]

Chan EC, Kuo SM, Kong AM, Morrison WA, Dusting GJ, Mitchell GM, Lim SY, Liu GS (2016) Three Dimensional Collagen Scaffold Promotes Intrinsic Vascularisation for Tissue Engineering Applications. PloS one 11(2): e0149799.

Chen Y, Chen S, Kawazoe N, Chen G (2018) Promoted Angiogenesis and Osteogenesis by Dexamethasone-loaded Calcium Phosphate Nanoparticles/Collagen Composite Scaffolds with Microgroove Networks. Scientific reports 8(1): 14143. [PubMed: 30237563]

Chocholata P, Kulda V, Babuska V (2019) Fabrication of Scaffolds for Bone-Tissue Regeneration. Materials 12(4).

Cooper DKC, Ekser B, Tector AJ (2015) Immunobiological barriers to xenotransplantation. International journal of surgery 23(Pt B): 211–216. [PubMed: 26159291]

De Long WG Jr., Einhorn TA, Koval K, McKee M, Smith W, Sanders R, Watson T (2007) Bone grafts and bone graft substitutes in orthopaedic trauma surgery. A critical analysis. The Journal of bone and joint surgery American volume 89(3): 649–658.

Fassbender M, Minkwitz S, Thiele M, Wildemann B (2014) Efficacy of two different demineralized bone matrix grafts to promote bone healing in a critical-size-defect: a radiological, histological and

histomorphometric study in rat femurs. International orthopaedics 38(9): 1963–1969. [PubMed: 24714881]

Feichtinger GA, Morton TJ, Zimmermann A, Dopler D, Banerjee A, Redl H, van Griensven M (2011) Enhanced reporter gene assay for the detection of osteogenic differentiation. Tissue engineering Part C, Methods 17(4): 401–410. [PubMed: 21043997]

Fielding G, Bose S (2013) SiO2 and ZnO dopants in three-dimensionally printed tricalcium phosphate bone tissue engineering scaffolds enhance osteogenesis and angiogenesis in vivo. Acta biomaterialia 9(11): 9137–9148. [PubMed: 23871941]

Fu C, Yang X, Tan S, Song L (2017) Enhancing Cell Proliferation and Osteogenic Differentiation of MC3T3-E1 Pre-osteoblasts by BMP-2 Delivery in Graphene Oxide-Incorporated PLGA/HA Biodegradable Microcarriers. Scientific reports 7(1): 12549.

Giannoni P, Scaglione S, Daga A, Ilengo C, Cilli M, Quarto R (2010) Short-time survival and engraftment of bone marrow stromal cells in an ectopic model of bone regeneration. Tissue engineering Part A 16(2): 489–499. [PubMed: 19712045]

Grosso A, Burger MG, Lunger A, Schaefer DJ, Banfi A, Di Maggio N (2017) It Takes Two to Tango: Coupling of Angiogenesis and Osteogenesis for Bone Regeneration. Frontiers in bioengineering and biotechnology 5: 68. [PubMed: 29164110]

Han B, Tang B, Nimni ME (2003) Quantitative and sensitive in vitro assay for osteoinductive activity of demineralized bone matrix. Journal of orthopaedic research : official publication of the Orthopaedic Research Society 21(4): 648–654. [PubMed: 12798064]

Hashimoto Y, Funamoto S, Kimura T, Nam K, Fujisato T, Kishida A (2011) The effect of decellularized bone/bone marrow produced by high-hydrostatic pressurization on the osteogenic differentiation of mesenchymal stem cells. Biomaterials 32(29): 7060–7067. [PubMed: 21724252]

Heo SY, Ko SC, Nam SY, Oh J, Kim YM, Kim JI, Kim N, Yi M, Jung WK (2018) Fish bone peptide promotes osteogenic differentiation of MC3T3-E1 pre-osteoblasts through upregulation of MAPKs and Smad pathways activated BMP-2 receptor. Cell biochemistry and function 36(3): 137–146. [PubMed: 29392739]

Hesami P, Holzapfel BM, Taubenberger A, Roudier M, Fazli L, Sieh S, Thibaudeau L, Gregory LS, Hutmacher DW, Clements JA (2014) A humanized tissue-engineered in vivo model to dissect interactions between human prostate cancer cells and human bone. Clinical & experimental metastasis 31(4): 435–446. [PubMed: 24510218]

Hirata A, Ueno T, Moy PK (2017) Newly Formed Bone Induced by Recombinant Human Bone Morphogenetic Protein-2: A Histological Observation. Implant dentistry 26(2): 173–177. [PubMed: 28207598]

Hsu EL, Ghodasra JH, Ashtekar A, Nickoli MS, Lee SS, Stupp SI, Hsu WK (2013) A comparative evaluation of factors influencing osteoinductivity among scaffolds designed for bone regeneration. Tissue engineering Part A 19(15–16): 1764–1772. [PubMed: 23521090]

Hupkes M, Sotoca AM, Hendriks JM, van Zoelen EJ, Dechering KJ (2014) MicroRNA miR-378 promotes BMP2-induced osteogenic differentiation of mesenchymal progenitor cells. BMC Mol Biol 15(1): 1. [PubMed: 24467925]

Iaquinta MR, Mazzoni E, Manfrini M, D'Agostino A, Trevisiol L, Nocini R, Trombelli L, Barbanti-Brodano G, Martini F, Tognon M (2019) Innovative Biomaterials for Bone Regrowth. International journal of molecular sciences 20(3).

Kanayama S, Kaito T, Kitaguchi K, Ishiguro H, Hashimoto K, Chijimatsu R, Otsuru S, Takenaka S, Makino T, Sakai Y, Myoui A, Yoshikawa H (2017) ONO-1301 Enhances in vitro Osteoblast Differentiation and in vivo Bone Formation Induced by Bone Morphogenetic Protein. Spine.

Katagiri T, Yamaguchi A, Komaki M, Abe E, Takahashi N, Ikeda T, Rosen V, Wozney JM, Fujisawa-Sehara A, Suda T (1994) Bone morphogenetic protein-2 converts the differentiation pathway of C2C12 myoblasts into the osteoblast lineage. J Cell Biol 127(6 Pt 1): 1755–1766. [PubMed: 7798324]

Kerr BA, McCabe NP, Feng W, Byzova TV (2013) Platelets govern pre-metastatic tumor communication to bone. Oncogene 32(36): 4319–4324. [PubMed: 23069656]

Khan SN, Cammisa FP Jr., Sandhu HS, Diwan AD, Girardi FP, Lane JM (2005) The biology of bone grafting. The Journal of the American Academy of Orthopaedic Surgeons 13(1): 77–86. [PubMed: 15712985]

Kolambkar YM, Dupont KM, Boerckel JD, Huebsch N, Mooney DJ, Hutmacher DW, Guldberg RE (2011) An alginate-based hybrid system for growth factor delivery in the functional repair of large bone defects. Biomaterials 32(1): 65–74. [PubMed: 20864165]

Kouroupis D, Baboolal TG, Jones E, Giannoudis PV (2013) Native multipotential stromal cell colonization and graft expander potential of a bovine natural bone scaffold. Journal of orthopaedic research : official publication of the Orthopaedic Research Society.

Liu G, Sun J, Li Y, Zhou H, Cui L, Liu W, Cao Y (2008) Evaluation of partially demineralized osteoporotic cancellous bone matrix combined with human bone marrow stromal cells for tissue engineering: an in vitro and in vivo study. Calcified tissue international 83(3): 176–185. [PubMed: 18704250]

Liu Y, Moller B, Wiltfang J, Warnke PH, Terheyden H (2014) Tissue engineering of a vascularized bone graft of critical size with an osteogenic and angiogenic factor-based in vivo bioreactor. Tissue engineering Part A 20(23–24): 3189–3197. [PubMed: 24919114]

Livak KJ, Schmittgen TD (2001) Analysis of relative gene expression data using real-time quantitative PCR and the 2(-Delta Delta C(T)) Method. Methods (San Diego, Calif) 25(4): 402–408.

Lu X, Wang J, Li B, Zhang Z, Zhao L (2013) Gene expression profile study on osteoinductive effect of natural hydroxyapatite. J Biomed Mater Res A.

Marcos-Campos I, Marolt D, Petridis P, Bhumiratana S, Schmidt D, Vunjak-Novakovic G (2012) Bone scaffold architecture modulates the development of mineralized bone matrix by human embryonic stem cells. Biomaterials 33(33): 8329–8342. [PubMed: 22901965]

McCabe NP, Kerr BA, Madajka M, Vasanji A, Byzova TV (2011) Augmented osteolysis in SPARC-deficient mice with bone-residing prostate cancer. Neoplasia 13(1): 31–39. [PubMed: 21245938]

Miron RJ, Saulacic N, Buser D, Iizuka T, Sculean A (2013) Osteoblast proliferation and differentiation on a barrier membrane in combination with BMP2 and TGFbeta1. Clinical oral investigations 17(3): 981–988. [PubMed: 22669486]

Muschler GF, Nakamoto C, Griffith LG (2004) Engineering principles of clinical cell-based tissue engineering. The Journal of bone and joint surgery American volume 86-A(7): 1541–1558.

Nakai T, Yoshimura Y, Deyama Y, Suzuki K, Iida J (2009) Mechanical stress up-regulates RANKL expression via the VEGF autocrine pathway in osteoblastic MC3T3-E1 cells. Molecular medicine reports 2(2): 229–234. [PubMed: 21475817]

Oryan A, Alidadi S, Moshiri A, Maffulli N (2014) Bone regenerative medicine: classic options, novel strategies, and future directions. Journal of orthopaedic surgery and research 9(1): 18. [PubMed: 24628910]

Oryan A, Kamali A, Moshiri A, Baghaban Eslaminejad M (2017) Role of Mesenchymal Stem Cells in Bone Regenerative Medicine: What Is the Evidence? Cells, tissues, organs 204(2): 59–83. [PubMed: 28647733]

Pearson HB, Mason DE, Kegelman CD, Zhao L, Dawahare JH, Kacena MA, Boerckel JD (2019) Effects of Bone Morphogenetic Protein-2 on Neovascularization During Large Bone Defect Regeneration. Tissue engineering Part A.

Pierson RN 3rd, Dorling A, Ayares D, Rees MA, Seebach JD, Fishman JA, Hering BJ, Cooper DK (2009) Current status of xenotransplantation and prospects for clinical application. Xenotransplantation 16(5): 263–280. [PubMed: 19796067]

Pina S, Canadas RF, Jimenez G, Peran M, Marchal JA, Reis RL, Oliveira JM (2017) Biofunctional Ionic-Doped Calcium Phosphates: Silk Fibroin Composites for Bone Tissue Engineering Scaffolding. Cells, tissues, organs 204(3–4): 150–163. [PubMed: 28803246]

Polo-Corrales L, Latorre-Esteves M, Ramirez-Vick JE (2014) Scaffold design for bone regeneration. Journal of nanoscience and nanotechnology 14(1): 15–56. [PubMed: 24730250]

Qadir AS, Um S, Lee H, Baek K, Seo BM, Lee G, Kim GS, Woo KM, Ryoo HM, Baek JH (2015) miR-124 negatively regulates osteogenic differentiation and in vivo bone formation of mesenchymal stem cells. J Cell Biochem 116(5): 730–742. [PubMed: 25424317]

Reichert JC, Cipitria A, Epari DR, Saifzadeh S, Krishnakanth P, Berner A, Woodruff MA, Schell H, Mehta M, Schuetz MA, Duda GN, Hutmacher DW (2012) A tissue engineering solution forsegmental defect regeneration in load-bearing long bones. Science translational medicine 4(141): 141–193.

Roddy E, DeBaun MR, Daoud-Gray A, Yang YP, Gardner MJ (2018) Treatment of critical-sized bone defects: clinical and tissue engineering perspectives. European journal of orthopaedic surgery & traumatology : orthopedie traumatologie 28(3): 351–362. [PubMed: 29080923]

Saran U, Gemini Piperni S, Chatterjee S (2014) Role of angiogenesis in bone repair. Archives of biochemistry and biophysics 561: 109–117. [PubMed: 25034215]

Seyler TM, Bracey DN, Plate JF, Lively MO, Mannava S, Smith TL, Saul JM, Poehling GG, Van Dyke ME, Whitlock PW (2017) The Development of a Xenograft-Derived Scaffold for Tendon and Ligament Reconstruction Using a Decellularization and Oxidation Protocol. Arthroscopy : the journal of arthroscopic & related surgery : official publication of the Arthroscopy Association of North America and the International Arthroscopy Association 33(2): 374–386.

Shahi M, Nadari M, Sahmani M, Seyedjafari E, Ahmadbeigi N, Peymani A (2018) Osteoconduction of Unrestricted Somatic Stem Cells on an Electrospun Polylactic-Co-Glycolic Acid Scaffold Coated with Nanohydroxyapatite. Cells, tissues, organs 205(1): 9–19. [PubMed: 29414820]

Sharma S, Sapkota D, Xue Y, Rajthala S, Yassin MA, Finne-Wistrand A, Mustafa K (2018) Delivery of VEGFA in bone marrow stromal cells seeded in copolymer scaffold enhances angiogenesis, but is inadequate for osteogenesis as compared with the dual delivery of VEGFA and BMP2 in a subcutaneous mouse model. Stem cell research & therapy 9(1): 23. [PubMed: 29386057]

Shi K, Lu J, Zhao Y, Wang L, Li J, Qi B, Li H, Ma C (2013) MicroRNA-214 suppresses osteogenic differentiation of C2C12 myoblast cells by targeting Osterix. Bone 55(2): 487–494. [PubMed: 23579289]

Shi Q, Li Y, Sun J, Zhang H, Chen L, Chen B, Yang H, Wang Z (2012) The osteogenesis of bacterial cellulose scaffold loaded with bone morphogenetic protein-2. Biomaterials 33(28): 6644–6649. [PubMed: 22727467]

Shuang Y, Yizhen L, Zhang Y, Fujioka-Kobayashi M, Sculean A, Miron RJ (2016) In vitro characterization of an osteoinductive biphasic calcium phosphate in combination with recombinant BMP2. BMC oral health 17(1): 35. [PubMed: 27485617]

Shui W, Zhang W, Yin L, Nan G, Liao Z, Zhang H, Wang N, Wu N, Chen X, Wen S, He Y, Deng F, Zhang J, Luu HH, Shi LL, Hu Z, Haydon RC, Mok J, He TC (2013) Characterization of scaffold carriers for BMP9-transduced osteoblastic progenitor cells in bone regeneration. J Biomed Mater Res A.

Smith CA, Board TN, Rooney P, Eagle MJ, Richardson SM, Hoyland JA (2017) Human decellularized bone scaffolds from aged donors show improved osteoinductive capacity compared to young donor bone. PloS one 12(5): e0177416.

Smith CA, Richardson SM, Eagle MJ, Rooney P, Board T, Hoyland JA (2015) The use of a novel bone allograft wash process to generate a biocompatible, mechanically stable and osteoinductive biological scaffold for use in bone tissue engineering. Journal of tissue engineering and regenerative medicine 9(5): 595–604. [PubMed: 24945627]

Sondag GR, Salihoglu S, Lababidi SL, Crowder DC, Moussa FM, Abdelmagid SM, Safadi FF (2013) Osteoactivin Induces Transdifferentiation of C2C12 Myoblasts into Osteoblasts. J Cell Physiol.

Stegen S, van Gastel N, Carmeliet G (2015) Bringing new life to damaged bone: the importance of angiogenesis in bone repair and regeneration. Bone 70: 19–27. [PubMed: 25263520]

Stiehler M, Seib FP, Rauh J, Goedecke A, Werner C, Bornhauser M, Gunther KP, Bernstein P (2010) Cancellous bone allograft seeded with human mesenchymal stromal cells: a potential good manufacturing practice-grade tool for the regeneration of bone defects. Cytotherapy 12(5): 658–668. [PubMed: 20429788]

Sun P, Wang J, Zheng Y, Fan Y, Gu Z (2012) BMP2/7 heterodimer is a stronger inducer of bone regeneration in peri-implant bone defects model than BMP2 or BMP7 homodimer. Dental materials journal 31(2): 239–248. [PubMed: 22447058]

Thibault RA, Scott Baggett L, Mikos AG, Kasper FK (2010) Osteogenic differentiation of mesenchymal stem cells on pregenerated extracellular matrix scaffolds in the absence of

osteogenic cell culture supplements. Tissue engineering Part A 16(2): 431–440. [PubMed: 19863274]

Tokuda H, Adachi S, Matsushima-Nishiwaki R, Kato K, Natsume H, Otsuka T, Kozawa O (2011) Enhancement of basic fibroblast growth factor-stimulated VEGF synthesis by Wnt3a in osteoblasts. International journal of molecular medicine 27(6): 859–864. [PubMed: 21399861]

Tokuda H, Takai S, Hanai Y, Harada A, Matsushima-Nishiwaki R, Kato H, Ogura S, Kozawa O (2008) Potentiation by platelet-derived growth factor-BB of FGF-2-stimulated VEGF release in osteoblasts. Journal of bone and mineral metabolism 26(4): 335–341. [PubMed: 18600399]

Vadori M, Cozzi E (2015) The immunological barriers to xenotransplantation. Tissue antigens 86(4): 239–253. [PubMed: 26381044]

Wancket LM (2015) Animal Models for Evaluation of Bone Implants and Devices: Comparative Bone Structure and Common Model Uses. Vet Pathol 52(5): 842–850. [PubMed: 26163303]

Wang JH, Chen J, Kuo SM, Mitchell GM, Lim SY, Liu GS (2019) Methods for Assessing Scaffold Vascularization In Vivo. Methods in molecular biology 1993: 217–226. [PubMed: 31148090]

Wanschitz F, Stein E, Sutter W, Kneidinger D, Smolik K, Watzinger F, Turhani D (2007) Expression patterns of Ets2 protein correlate with bone-specific proteins in cell-seeded three-dimensional bone constructs. Cells, tissues, organs 186(4): 213–220. [PubMed: 17703088]

Whitlock PW, Seyler TM, Parks GD, Ornelles DA, Smith TL, Van Dyke ME, Poehling GG (2012) A novel process for optimizing musculoskeletal allograft tissue to improve safety, ultrastructural properties, and cell infiltration. The Journal of bone and joint surgery American volume 94(16): 1458–1467.

Whitlock PW, Smith TL, Poehling GG, Shilt JS, Van Dyke M (2007) A naturally derived, cytocompatible, and architecturally optimized scaffold for tendon and ligament regeneration. Biomaterials 28(29): 4321–4329. [PubMed: 17610948]

Yang Q, Jian J, Abramson SB, Huang X (2011) Inhibitory effects of iron on bone morphogenetic protein 2-induced osteoblastogenesis. J Bone Miner Res 26(6): 1188–1196. [PubMed: 21308772]

Yu S, Geng Q, Ma J, Sun F, Yu Y, Pan Q, Hong A (2013) Heparin-binding EGF-like growth factor and miR-1192 exert opposite effect on Runx2-induced osteogenic differentiation. Cell Death Dis 4: e868.

Zheng Y, Wang L, Zhang X, Zhang X, Gu Z, Wu G (2012) BMP2/7 heterodimer can modulate all cellular events of the in vitro RANKL-mediated osteoclastogenesis, respectively, in different dose patterns. Tissue engineering Part A 18(5–6): 621–630. [PubMed: 21981321]

Zheng ZW, Chen YH, Wu DY, Wang JB, Lv MM, Wang XS, Sun J, Zhang ZY (2018) Development of an Accurate and Proactive Immunomodulatory Strategy to Improve Bone Substitute Material-Mediated Osteogenesis and Angiogenesis. Theranostics 8(19): 5482–5500. [PubMed: 30555559]

Zhu W, Rawlins BA, Boachie-Adjei O, Myers ER, Arimizu J, Choi E, Lieberman JR, Crystal RG, Hidaka C (2004) Combined bone morphogenetic protein-2 and −7 gene transfer enhances osteoblastic differentiation and spine fusion in a rodent model. Journal of bone and mineral research : the official journal of the American Society for Bone and Mineral Research 19(12): 2021–2032.

Zimmermann G, Moghaddam A (2011) Allograft bone matrix versus synthetic bone graft substitutes. Injury 42 Suppl 2: S16–21. [PubMed: 21889142]

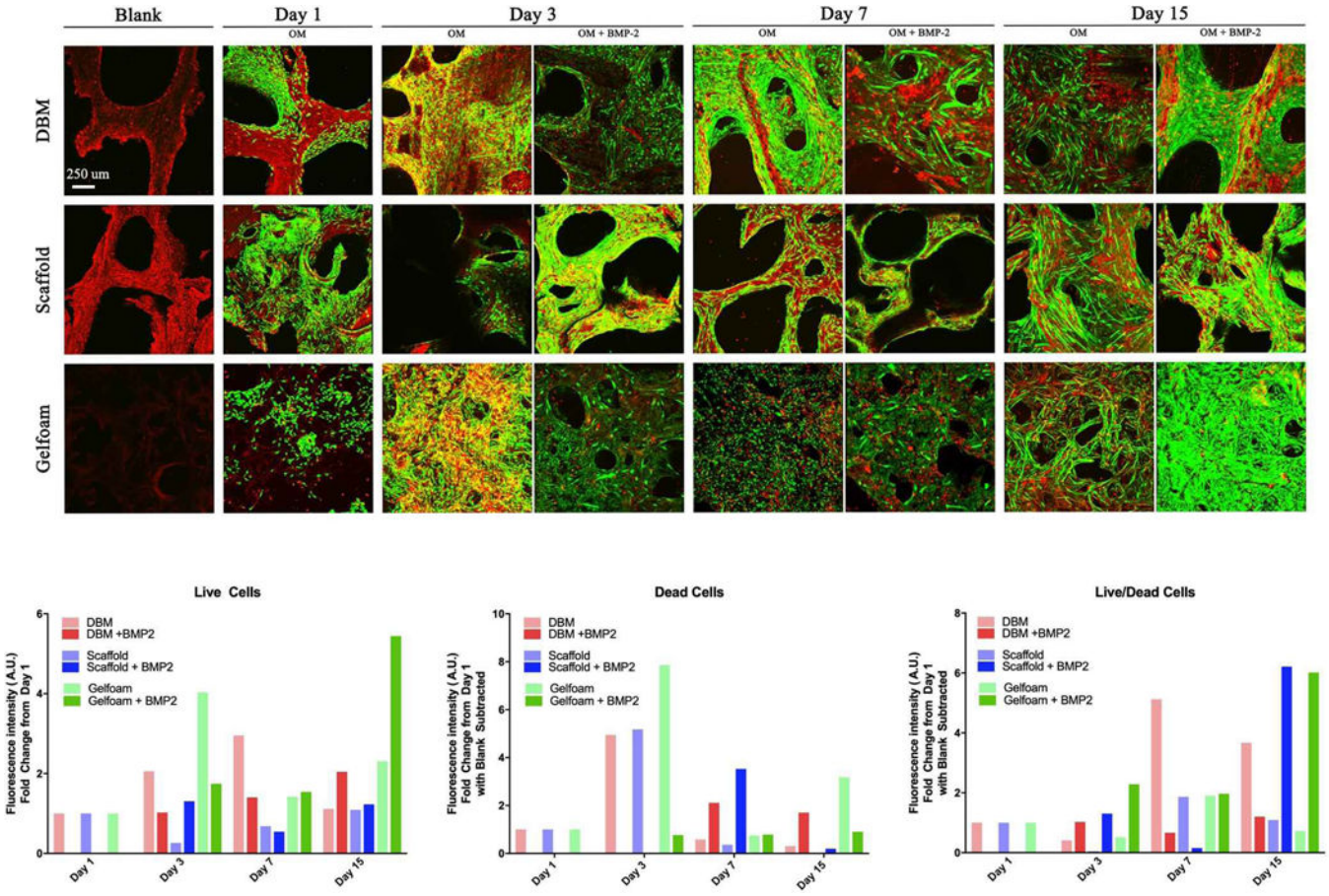

Figure 1. C2C12 cells are viable on the decellularized bone scaffold.

Demineralized Bone Matrix (DBM), scaffold, and gelfoam matrices were seeded with 1 million C2C12 pre-osteoblast cells, incubated for 1, 3, 7, or 15 days. On day 1, matrices were switched into osteogenic media (OM) enriched with 100 ng/mL BMP-2. Representative micrographs show green fluorophore (calcein AM) staining of live cells and red fluorophore (ethidium) staining of dead cells. Constructs had notable autofluorescence with ethidium staining as shown in the “blank” images. Cross-sectional images were captured at 10X magnification and overlaid to create the shown 3D projections. Cell density increased with time on all three matrices, consistent with DNA quantification results. Fluorescence in each channel was quantified and represented as fold change in fluorescence intensity from Day 1 ± SD.

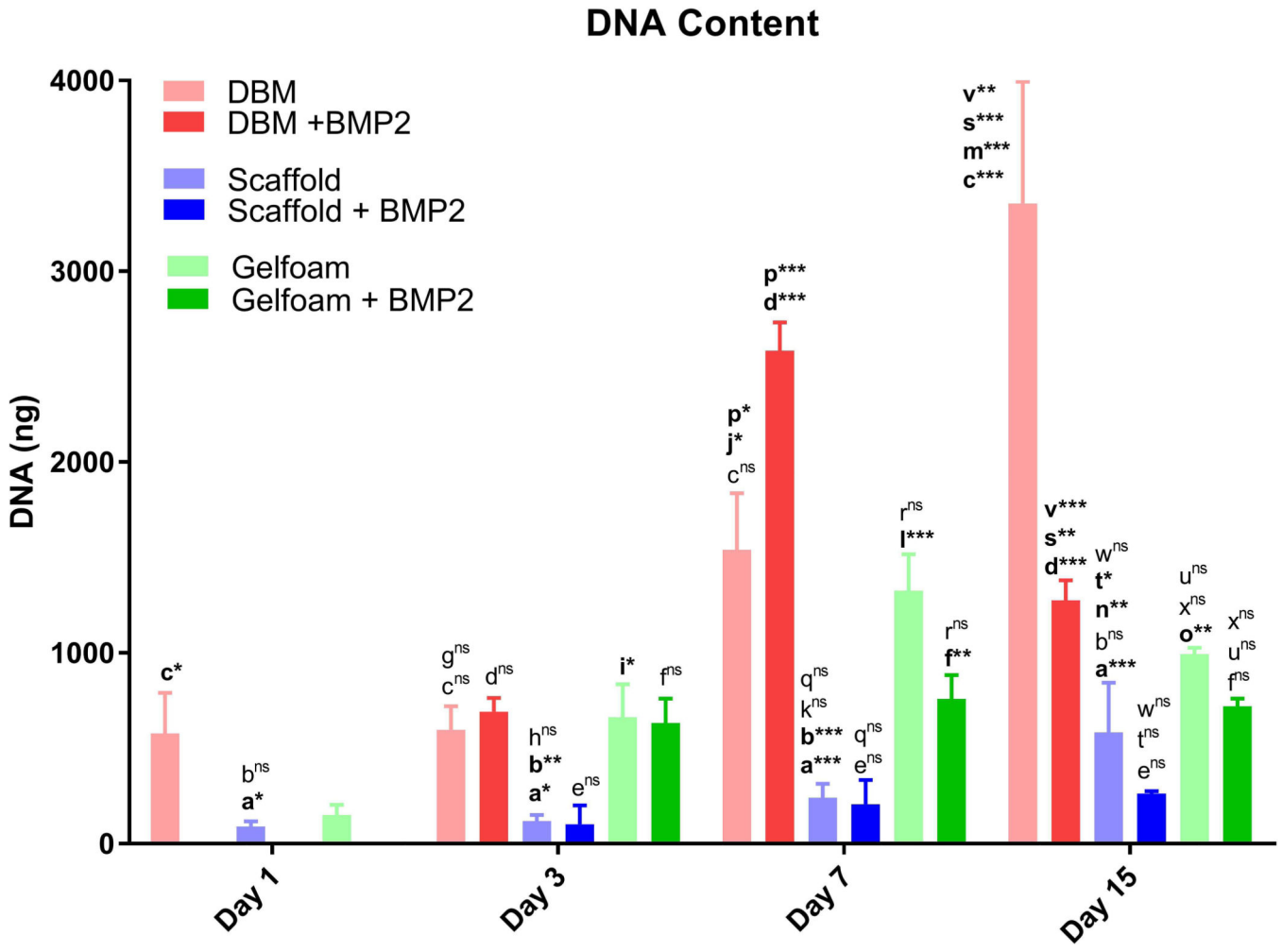

Figure 2. C2C12 cells proliferate slowly on the decellularized bone constructs.

DBM (red bars), bone scaffold (blue bars), or gelfoam (green bars) constructs were treated with control media, osteogenic media (OM), or OM with 100 ng/mL BMP-2 starting on day 2. Constructs were harvested at days 1, 3, 7, and 15, DNA content was measured with the PicoGreen® assay, and represented as mean DNA mass ± SD. * represents $p<0.05$, ** represents <0.01, and *** represents $p<0.001$ by two-way ANOVA for construct and treatment and one-way ANOVA for time within each construct and treatment. Comparisons are annotated as below:

(**a**) scaffold vs DBM; (**b**) scaffold vs gelfoam; (**c**) DBM vs gelfoam

(**d**) DBM OM vs OM + BMP-2; (**e**) scaffold OM vs OM + BMP-2 (**f**) gelfoam OM vs OM + BMP-2;

(**g**) DBM day 1 vs 3; (**h**) scaffold day 1 vs 3; (**i**) gelfoam day 1 vs 3;

(**j**) DBM day 1 vs 7; (**k**) scaffold day 1 vs 7; (**l**) gelfoam day 1 vs 7;

(**m**) DBM day 1 vs 15; (**n**) scaffold day 1 vs 15; (**o**) gelfoam day 1 vs 15;

(**p**) DBM day 3 vs 7; (**q**) scaffold day 3 vs 7; (**r**) gelfoam day 3 vs 7

(**s**) DBM day 3 vs 15; (**t**) scaffold day 3 vs 15; (**u**) gelfoam day 3 vs 15

(**v**) DBM day 7 vs 15; (**w**) scaffold day 7 vs 15; (**x**) gelfoam day 7 vs 15

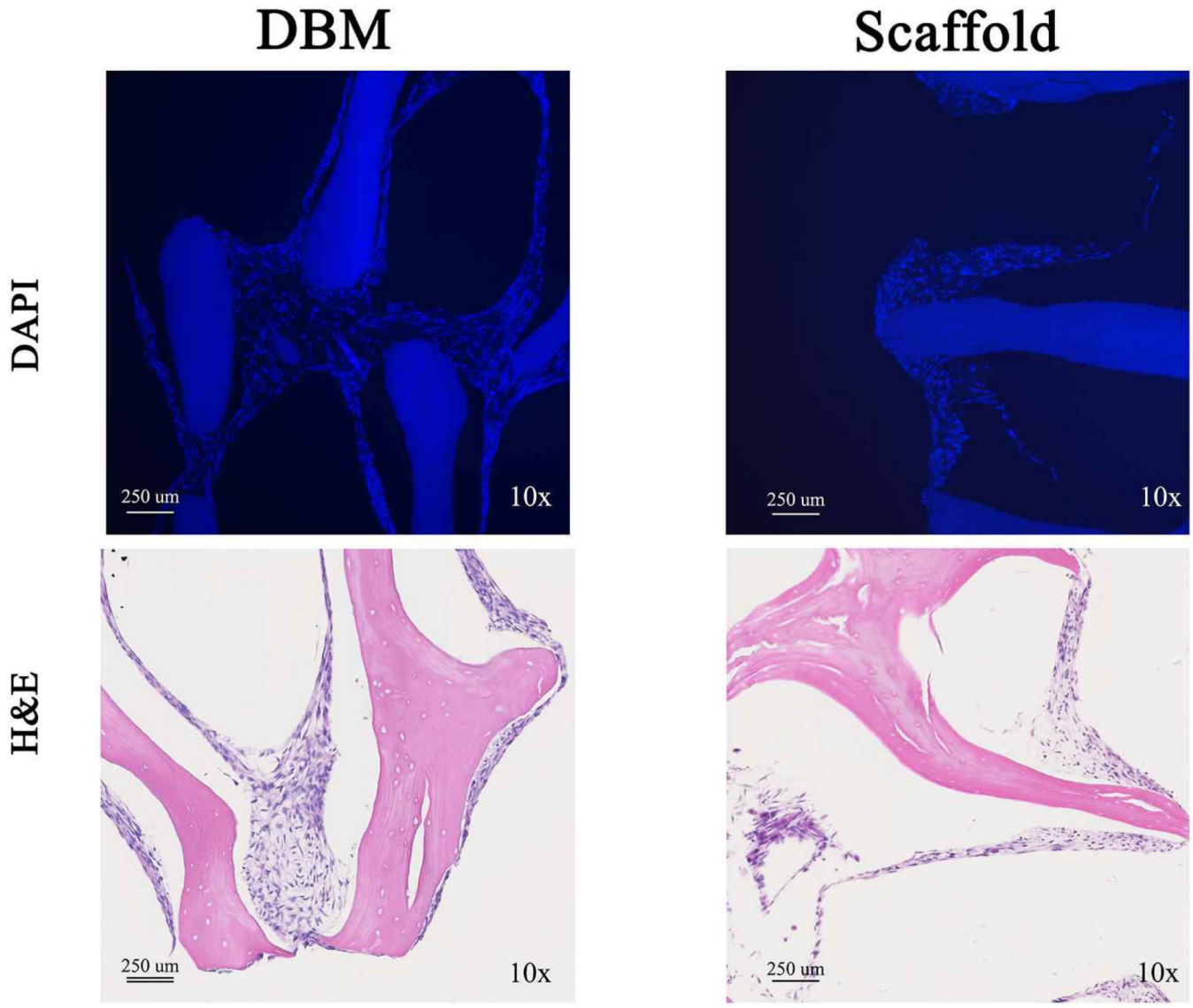

Figure 3. C2C12 cell density is increased on DBM compared with scaffolds.

C2C12 cells were seeded on DBM (left panels) or decellularized bone scaffold (right panels). Seeded scaffolds were sectioned and stained for DAPI (top panels) or H&E (bottom panels). Representative images are shown taken at 10X.

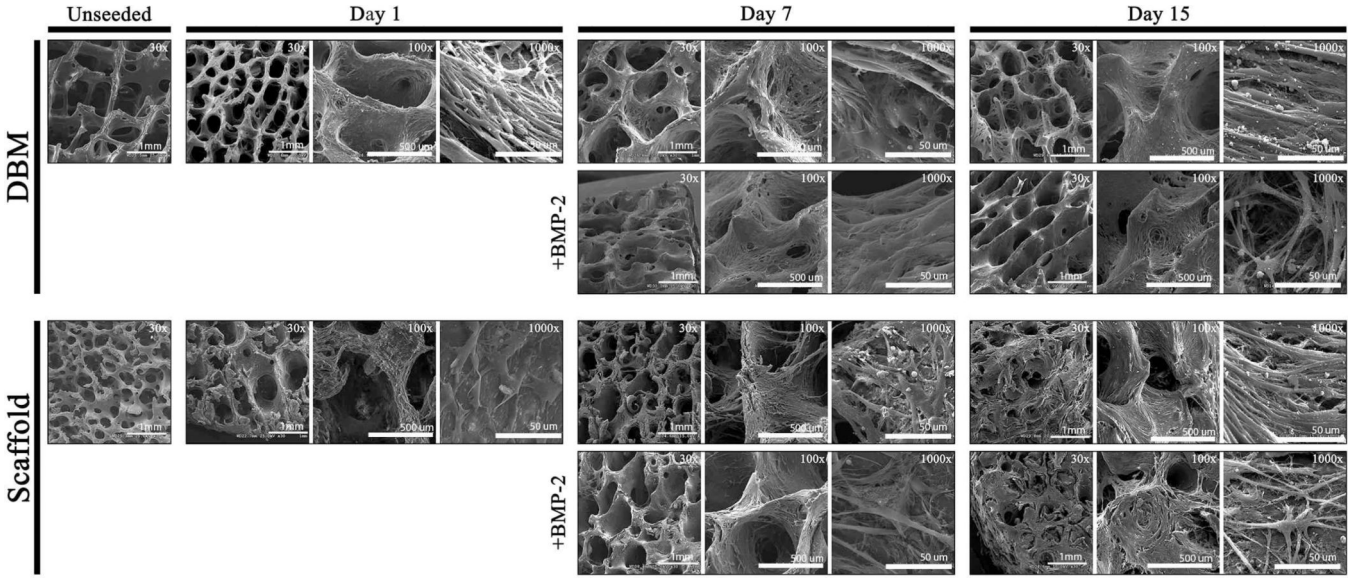

Figure 4. C2C12 attachment and spreading is equivalent on bone scaffolds and DBM

C2C12-seeded DBM and bone scaffolds were analyzed by scanning electron microscopy at days 1, 7, or 15 and compared to unseeded scaffolds. Comparison with 100 ng/mL BMP-2 treated scaffolds are shown. Representative images at 30X (scale bar represents 1 mm), 100X (scale bar represents 500 μm), and 1000X (scale bar represents 50 μm) are shown.

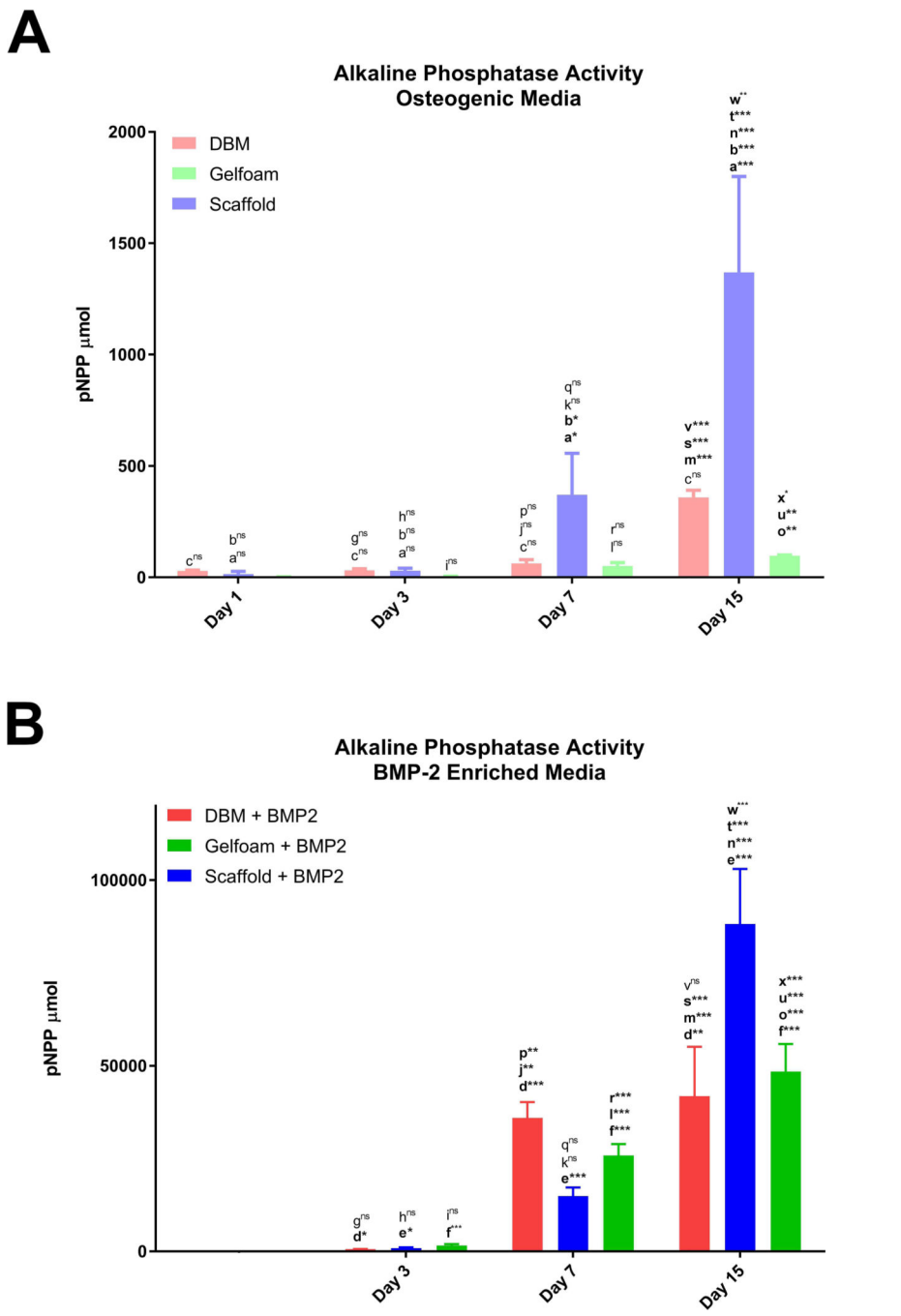

Figure 5. Scaffolds induce ALP activity in C2C12 cells.

C2C12-seeded constructs: DBM (red bars), bone scaffolds (blue bars), or Gelfoam (green bars), were incubated in osteogenic media (A) or in the presence of 100 ng/mL BMP-2 (B) with treatments starting on day 2 and analyzed for enzymatic ALP activity represented as mean total p-nitrophenyl phosphate (pNPP) content ± SD. * represents $p<0.05$, ** represents <0.01, and *** represents $p<0.001$ by two-way ANOVA for construct and treatment and one-way ANOVA for time within each construct and treatment. Comparisons are annotated as described below:

(**a**) scaffold vs DBM; (**b**) scaffold vs gelfoam; (**c**) DBM vs gelfoam
(**d**) DBM OM vs OM + BMP-2; (**e**) scaffold OM vs OM + BMP-2 (**f**) gelfoam OM vs OM + BMP-2;
(**g**) DBM day 1 vs 3; (**h**) scaffold day 1 vs 3; (**i**) gelfoam day 1 vs 3;
(**j**) DBM day 1 vs 7; (**k**) scaffold day 1 vs 7; (**l**) gelfoam day 1 vs 7;
(**m**) DBM day 1 vs 15; (**n**) scaffold day 1 vs 15; (**o**) gelfoam day 1 vs 15;
(**p**) DBM day 3 vs 7; (**q**) scaffold day 3 vs 7; (**r**) gelfoam day 3 vs 7
(**s**) DBM day 3 vs 15; (**t**) scaffold day 3 vs 15; (**u**) gelfoam day 3 vs 15
(**v**) DBM day 7 vs 15; (**w**) scaffold day 7 vs 15; (**x**) gelfoam day 7 vs 15

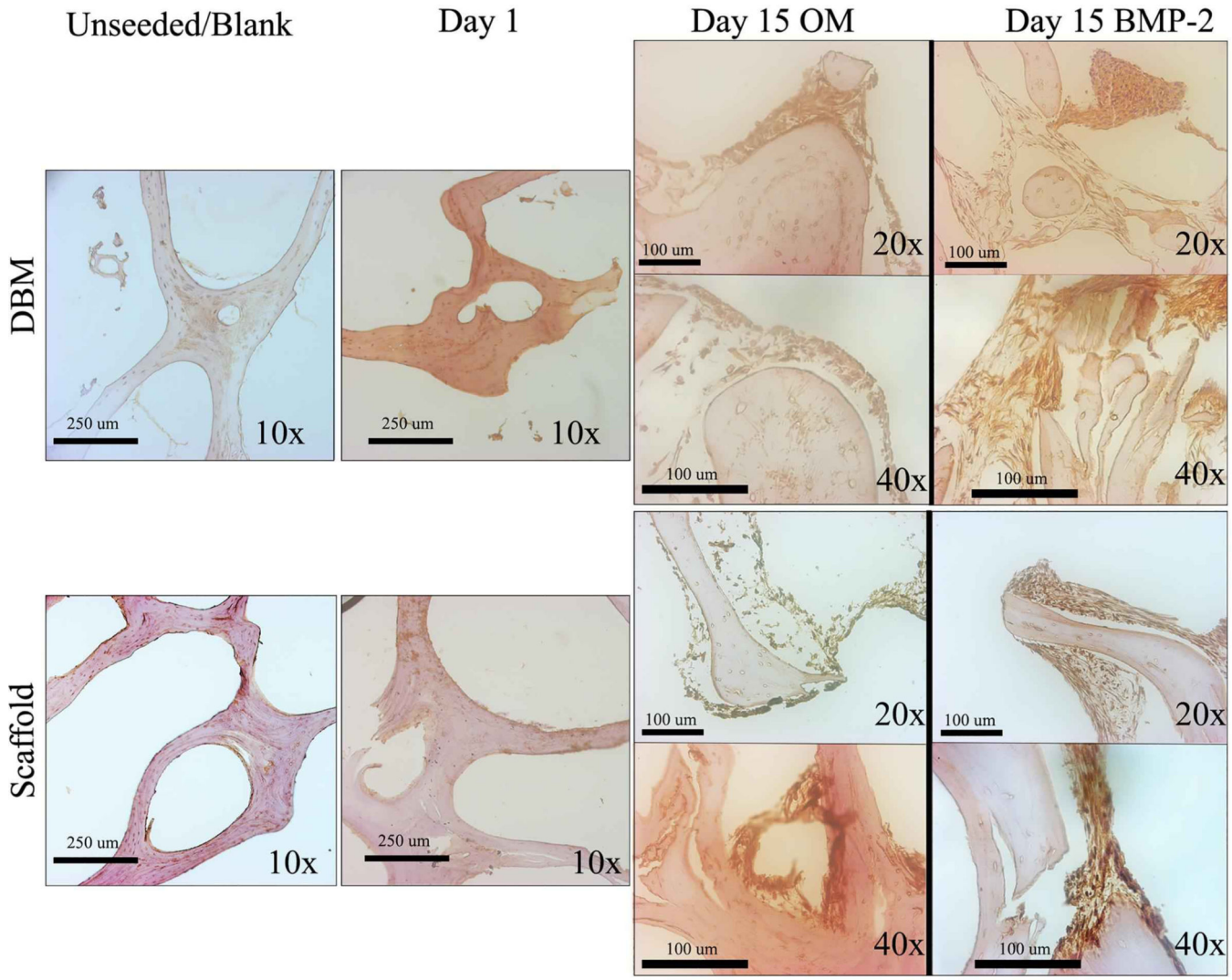

Figure 6. ALP expression increases over time in both DBM and scaffolds.

DBM (top panels) or decellularized bone (bottom panels) scaffolds were sectioned unseeded, after 1-day culture of C2C12 cells or after 15 days in OM or OM with 100 ng/mL BMP-2. Sections were stained for ALP expression by immunohistochemistry, and representative images are shown at 10X, 20X, and 40X. Images were taken at different locations and did not represent subsets of each other.

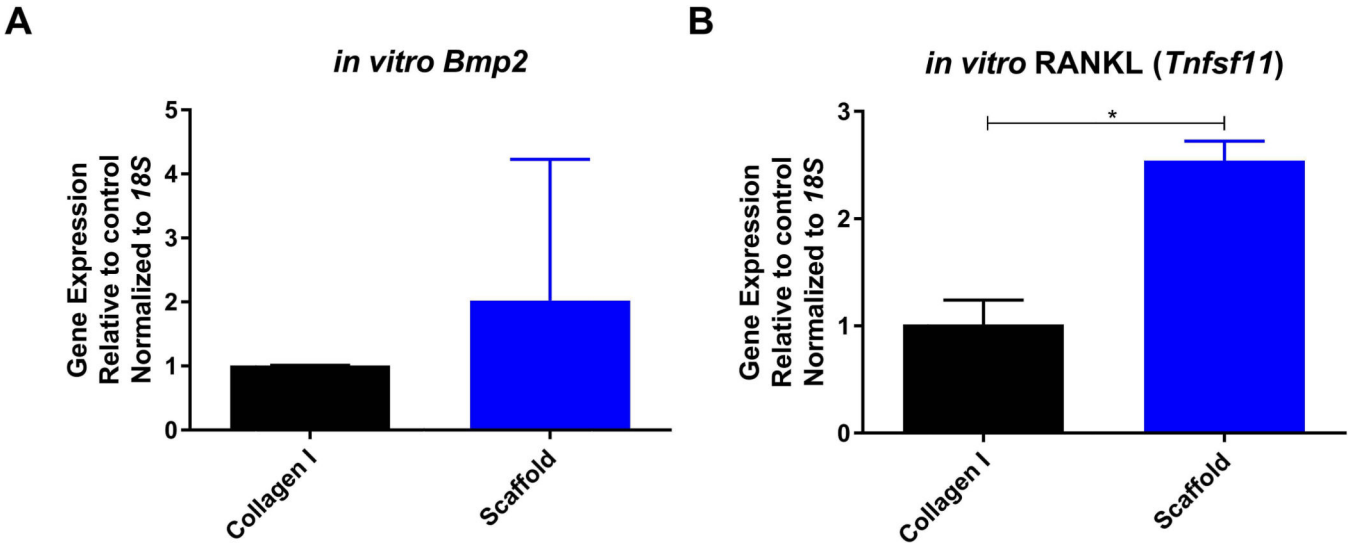

Figure 7. Scaffolds induce MC3T3-E1 osteogenic differentiation.

MC3T3-E1 cells were seeded on 10 μg/mL collagen I (black bars) or decellularized bone scaffolds (blue bars) for one week. Gene expression of *Bmp2* (A) and RANKL (*Tnsfs11*) (B) were measured and represented as mean fold change normalized to *18S* ± SD. * represents $p<0.05$ by t-test.

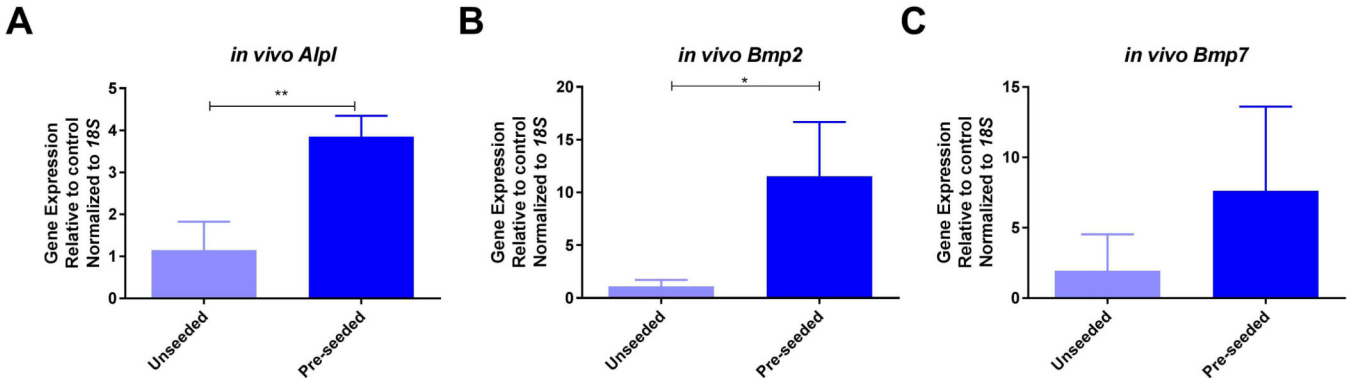

Figure 8. Implantation of scaffolds *in vivo* induces osteogenic gene expression.

Bone scaffolds were seeded with MC3T3-E1 pre-osteoblast cells (light blue bars) or left unseeded (dark blue bars) and implanted subcutaneously in syngeneic mice. After four weeks scaffolds were removed, processed, and analyzed for gene expression of ALP (*Alpl*) (A), *Bmp2* (B), and *Bmp7* (C) represented as mean fold change normalized to *18S* ± SD. * represents $p<0.05$ by t-test.

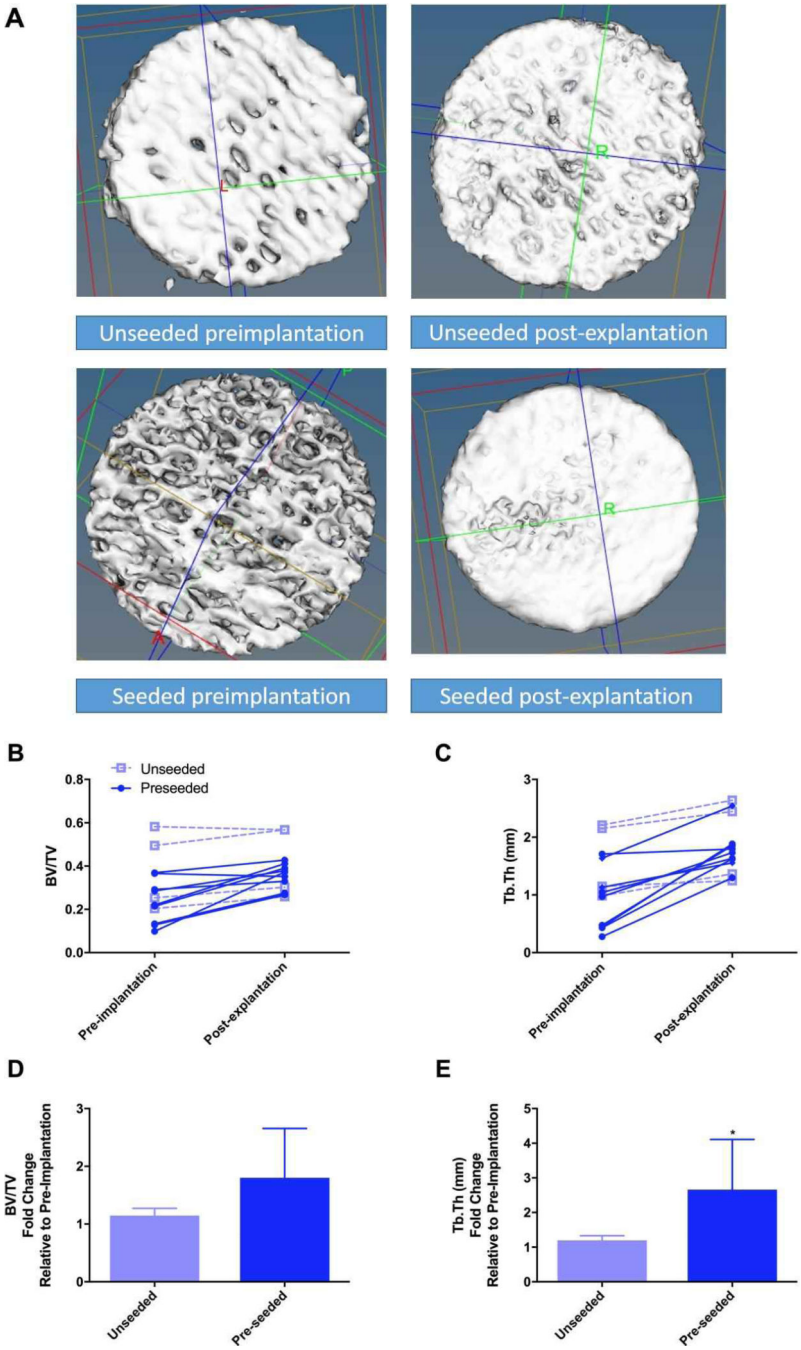

Figure 9. New bone formation occurs in implanted bone constructs.

Bone scaffold structure was analyzed by microCT (pre-implantation) and then implanted subcutaneously in mice either unseeded (open squares) or pre-seeded with MC3T3-E1 pre-osteoblast cells (closed circles). Representative microCT 3D projections of the bone scaffolds prior to implantation (left) and after explantation (right) from unseeded (top row) and seeded (bottom row), grossly demonstrating an appearance of bone formation are shown in A. Implants were removed after four weeks and scanned again by microCT (post-explantation). Bone volume ratio (BV/TV, B) and trabecular thickness (Tb.Th, C) were

calculated, and the change between individual scaffolds is shown. Fold change in BV/TV (D) and Tb.Th (E) are shown for unseeded (light blue bars) and preseeded (dark blue bars) as mean ± SD. * represents $p<0.05$ by paired t-test.

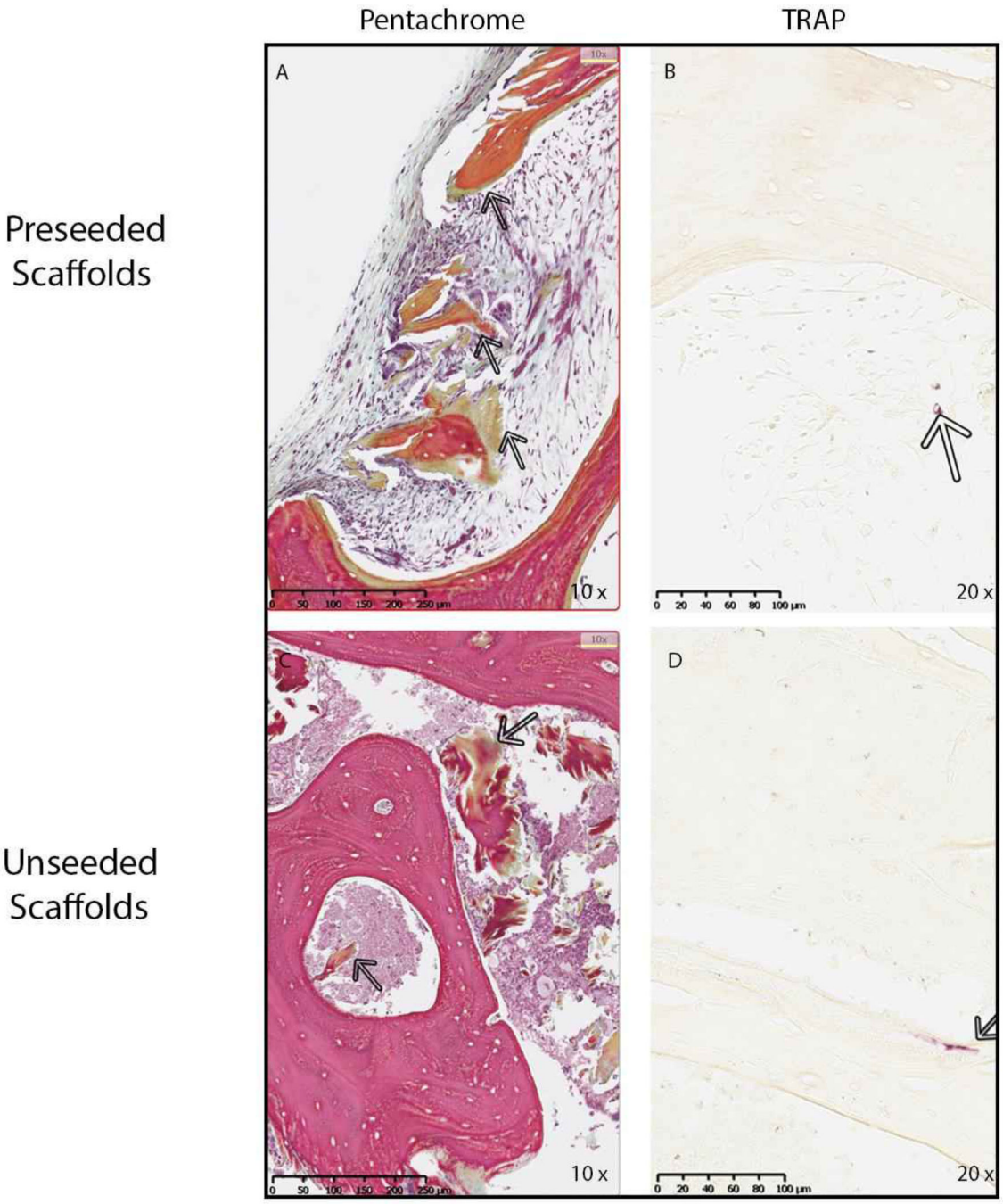

Figure 10. Implantation of bone scaffolds induces a functional bone microenvironment.

MC3T3-E1 seeded and unseeded scaffolds were removed from mice after four weeks and processed for histology. Sections were stained with Movat's pentachrome (A and C) to visualize the extracellular matrix deposition in the scaffolds. Arrows show the area of new bone formation in scaffold which stains green in representative photos captured at 10X. (B and D) Sections were also stained for osteoclasts using TRAP enzyme activity. Arrows point to purple staining demonstrating small TRAP-positive cells in the pores and along the bone surface in representative photos taken at 20X.

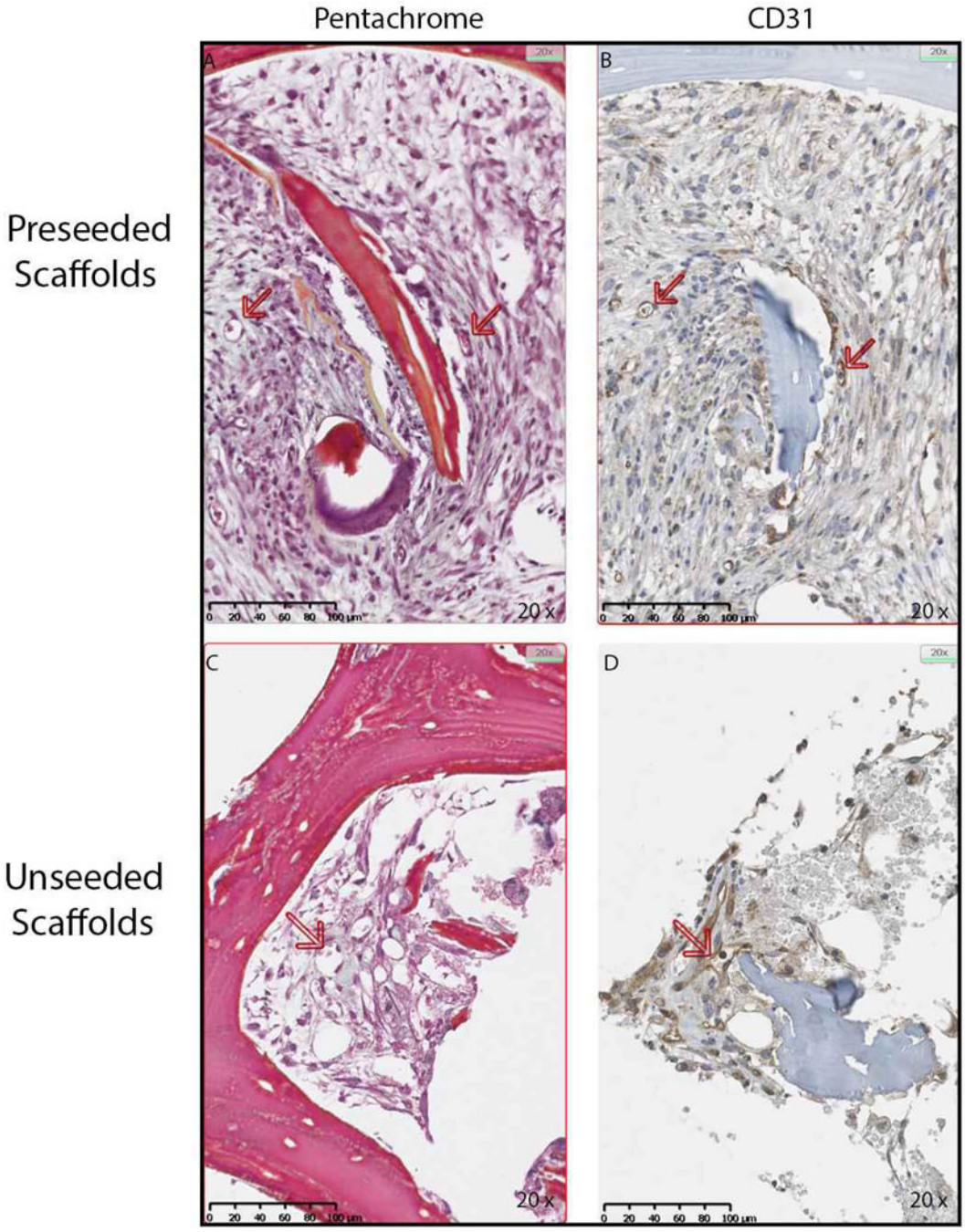

Figure 11. Angiogenesis occurs in the implanted bone scaffolds

MC3T3-E1 seeded and unseeded scaffolds were removed from mice after four weeks and processed for immunohistochemistry (IHC) for the endothelial marker CD31. In the representative micrographs at 20X, Movat's pentachrome (A and C) demonstrate small vessels indicated with arrows, and corresponding IHC for CD31 confirms that these are endothelial cells (B and D).

Table 1.

qPCR primer sequences

Primer	Sequence
Alkaline Phosphatase (forward)	GGCAGCGTCAGATGTTAATTG
Alkaline Phosphatase (reverse)	ACTGCGCTCCTTAGGGCT
Bone Morphogenetic Protein-7 (forward)	CTTGGAAAGATCAAACCGGA
Bone Morphogenetic Protein-7 (reverse)	GGACAGCCACTTCCTCACTG
Bone Morphogenetic Protein-2 (forward)	GAAGTTCCTCCACGGCTTCT
Bone Morphogenetic Protein-2 (reverse)	AGATCTGTACCGCAGGCACT
Receptor activator of nuclear factor κ B ligand (forward)	AGGCTGGGCCAAGATCTCTA
Receptor activator of nuclear factor κ B ligand (reverse)	GTCTGTAGGTACGCTTCCCG
18s (forward)	GCGGTTCTATTTTGTTGGTTT
18s (reverse)	CTCCGACTTTCGTTCTTGATT